STUDY OF AERODYNAMIC INTERFERENCE BETWEEN AXISYMMETRIC BODIES IN INCOMPRESSIBLE FLOWS BY THE METHOD OF INTERNAL SINGULARITIES

by

RAM KRISHAN CHAUHAN

DEPARTMENT OF AERONAUTICAL ENGINEERING

INDIAN INSTITUTE OF TECHNOLOGY KANPUR

DECEMBER, 1986

STUDY OF AERODYNAMIC INTERFERENCE BETWEEN AXISYMMETRIC BODIES IN INCOMPRESSIBLE FLOWS BY THE METHOD OF INTERNAL SINGULARITIES

A Thesis Submitted
in Partial Fulfilment of the Requirements
for the Degree of
MASTER OF TECHNOLOGY

by

RAM KRISHAN CHAUHAN

to the

DEPARTMENT OF AERONAUTICAL ENGINEERING
INDIAN INSTITUTE OF TECHNOLOGY KANPUR
DECEMBER, 1986

CERTIFICATE

Certified that the thesis titled 'Study of aerodynamic interference between axisymmetric bodies in incompressible flows by the method of internal singularity' is a bonafide work carried out by Shri Ram Krishan Chauhan under my supervision. This has not been submitted for a degree elsewhere.

C.V.R. MURTI
Assistant Professor
Department of Aeronautical Engg.
Indian Institute of Technology,
Kanpur

Dec. 14, 1986

(i)

ACKNOWLEDGEMENT

There is a pleasure in learning. I had a great desire to study in a good institution for the sake of learning pleasure. That long standing desire has now been fulfilled. I must acknowledge my gratitude to IIT, Kanpur for providing me excellent opportunity for learning and development. I am specially thankful to Prof. C.V.R. Murti for initiating me into this work, invaluable guidance and practical suggestions. This work would not have been complete without his roving observations at results for proper inferences and elimination of errors. I avail this opportunity to thank my colleagues, Shri P.K. Pandey, Shri Umesh Singh, Shri Prabhakaran and Shri R. Mahadevan for their useful help in my work. I am thankful to Shri J.C. Verma for his assistance in drawing figures and Shri S.J. Gupta for typing my thesis and Shri C.K. Awasthi for his help in general.

Rkchauhan.

RAM KRISHAN CHAUHAN

ABSTRACT

The problem of aerodynamic interference between axisymmetric bodies in inviscid, incompressible flow has been studied by separating the flow into axial flow and lateral flow. The problem of axial flow has been solved by representing isolated bodies in free stream by continuous source distribution of polynomial form along the axes of the bodies and the interfering flows by an additional continuous dipole distribution of polynomial form after Milne-Thompson's circle image theorem. The solution for the lateral flow is obtained by invoking slender body theory and using the method of two-dimensional multipole singularities (MPS). Flow tangency conditions over the surfaces of the body has been used for the axial flow problem, while constancy of stream function on the surfaces of the bodies has been used for the lateral flow. This method has been applied to study the interference between a pair of parabolic bodies of various thicknesses and for varying proximities. The perturbation velocities, the pressure distribution and the side force co-efficients and moments are computed and presented. This method of solving interference problem by using dipole distribution in axial flow and two-dimensional MPS in lateral flow appears to be a rapid and fairly accurate method for preliminary calculation of aerodynamic loads. This facilitates more efficient use of panel methods if required for greater accuracy.

CONTENTS

LIST OF SYMBOLS

a	nose spacing (distance of lateral separation between centres of two bodies)
A_n	Coefficient of strength for n_{th} order MPS(2D)
$A_{m(n)}, A_{1(\gamma)}$	Strength parameter, $A_{m(n)}=A_n \times M_n$
C_j, C_{dj}	Co-efficients of strength functions $f(\bar{x}), f_d(\bar{x})$ (3D)
Cp	Pressure co-efficient
C_{my}, C_{mz}	Moment co-efficient about nose in y dir. and z dir.
C_y, C_z	Side force co-efficients
FR	Fineness ratio
$f(\bar{x}), f_d(\bar{x})$	Strength distribution of sources and dipoles (3D)
ϕ	Velocity potential,
i,j,k	Unit vectors
L_n, M_n	Strength of n-th order MPS(2D) located at the centre of body 2 and body 1 respectively
N	Order of MPS (2D)
P	Field point
PR	Proximity ratio or spacing = $a/(r_1+r_2)$
x, r, θ,	Cylindrical polar co-ordinates
R	Distance P D of field point P from the singularity(3D)
r_1, r_2	Radii of circles C_1 and C_2.
r,	Radial distance from the axis for the field point P_i on body surface and of the delta line (3D)
r(x)	radius of body such that r(x) prescribes body surface.

r_{al}, r_{bl}	DB distance of the field point P. from the location of singularity at centre of 2nd body (2D)
ψ	Stream function (2D)
S_r	Ref. area at cross-section (3D)
τ (tau)	thickness ratio $(\frac{d_{max}}{l})$
$u_x, v_r, V_{\theta a}$	Perturbation velocity components in (x, r, θ) direction.
α, β	angle of incidence and yaw
$V_{\theta l}$, V_r	Tangential and radial velocity components in lateral flow.
$\bar{x}$	Dummy variable

Subscripts

d	dipole, doublet
s	singularity/source
q	quadrupole
o	octopole

LIST OF FIGURES

CHAPTER I

Introduction

This study is about aerodynamic ~~behaviour~~ interference of external stores and armaments carried by military aircraft . The interference could be between wing and the external stores, fuselage and external stores, or between the external stores themselves. The problem of interference between external stores, which are mostly axially symmetric bodies, has been taken up for the present study. The solution of this problem has been obtained by separating the 'axial flow' and the 'lateral flow'. The 'axial flow' solution is based on method of images and by a continuous source distribution, represented by a polynomial function, displaced from the axial line towards the interfering body. Lateral flow has been solved using slender body assumptions, treating the flow at various cross-sections along the axis as 2-dimensional. Multipole singularities like doublets quadrupoles etc. have been used for nullifying the cross-flow.

1.1 Motivation for the study

Modern military aircraft carry large amount of external stores and armaments like bombs, missiles, rockets and drop tanks under the wing and under the fuselage. Most of these stores are carried in close proximities to each other. There is considerable mutual interference of flow between these bodies. Proper knowledge of interference is necessary to calculate aerodynamic forces and moments

for safe carriage, launching and accurate delivery of these stores to their targets. An approximate, yet a rapid method of estimation of these effects is helpful in optimising and utilizing the available under the wing/fuselage area for maximum armament carrying capacity.

1.2 Literature Survey

The subject of flows past system of axi-symmetric bodies has been studied by many authors. Most of them have used singularities like sources, sinks, doublets and still higher derivatives of these singularities called multipoles to represent various shapes and bodies. These singularities could be distributed within the body or on the surface of the body. The former is called 'Internal Singularity' method and the latter 'Surface Singularity' method. The 'surface singularity' method is also related to the 'Panel method' wherein the surface is discretised into large number of panels. 'Panel method' is accurate but its accuracy depends on number of panels. So for greater accuracy, larger number of panels and hence larger computations are required. The method of internal singularity is simpler, rapid and reasonably accurate for smooth bodies.

The pioneering work in flows over axi-symmetric bodies was done by Rankine [1], who represented the axisymmetric body by source-sink pairs, along the axis of the body.

The bodies which may be represented by source-sink combinations are called 'Rankine bodies' or 'Rankine ovals', Von-Karman [2] represented a flow past body of revolution by continuous distribution of sources/sinks along the axis of the body. He used different source strength for different segments but the strength being constant over a particular element. For lateral flow he used continuous distribution of doublets, the doublets aligned opposite to the undisturbed lateral flow. James [3] obtained an analytic solution of velocity potential $\emptyset$ for flow over an axi-symmetric body by conformal mapping of the meridian profile of the body. He transformed meridian geometry of body into a circle and then approximated the velocity potential in terms of elementary functions such as Fourier Series, Legendre or Chebyshev polynomials. He obtained results which are comparable to those obtained by 'panel method.'

Zedan and Dalton [4] represented the body by parabolic variation of source strengths along axial segments of the body. By using 12 elements of source strengths each of 2 or 3 degree polynomial, they obtained accurate results for representing even thick bodies of fineness ratio upto 2, by iterative method. Their method is suitable for blunt nosed bodies also. Campbell [5] obtained least square solution of discrete distribution of sources along the axis.

His method is unsuitable for blunt bodies and also the number of sources required are large. Christopher and Shaw [6] used multi-polynomials of degrees 8 to 10 to represent bodies. They obtained accurate results for thick as well as blunt bodies.

Martin, Smith and Saunders [7] studied interference between two identical axi-symmetric bodies by using discrete distribution of sources for representing original bodies and using discrete distribution of dipoles along a displaced line which may be called image or delta line for the interfering flow. The drawback with discrete distribution of sources is that boundary conditions are satisfied at control points but there is a large error at points other than at control points, especially near nose or tail of the body. Christopher and Shaw [8] represented the bodies by multi-polynomials and used 3-dimensional multipole singularities (MPS) for the cross-flow due to the interference. They used MPS i.e. doublets, quadrupoles and octopoles each represented by polynomials of degree 8 to 10. This method has two drawbacks; firstly it has large number of unknown co-efficients (as large as 120) because of multi-polynomials and MPS.

1.3 Outline of the present work

In chapter 2, the axial flow problem is formulated. Continuous source distribution represented by 8-degree polynomial is used for isolated bodies. For interference an additional continuous distribution of dipole strength function represented by a 8 degree polynomial is used. The mathematical expressions of velocity potential ϕ and perturbation velocity components i.e. v_r, u_x, $V_{\theta a}$ are given along with governing equation and boundary conditions. The axial flow over a pair of axially-symmetric bodies, laterally separated, are studied for varying thickness ratios and proximities. Results are presented. In chapter 3, the lateral flow problem is formulated using slender body theory. The concept and application of 2-dimensional MPS, is explained. The mathematical expressions of stream function ψ and perturbation velocity components $V_{\theta 1}$ and V_r are given. Boundary conditions are also described. The two types of lateral flow viz., yawing and incident are solved separately and results are presented. The aerodynamic load distribution Cp, forces and moments are obtained.

In Chapter 4, the results are discussed. Limitations of discrete distribution of sources and factors responsible for error are stated. Suggestions for further extension and utilization of present work are given.

CHAPTER 2

Axial Flow

2.1 Potential flow solution

This chapter is devoted to analytic work and the mathematical formulations necessary to obtain solution of velocity potential ϕ, and to determine polynomial functions $f(\bar{x}), f_c(\bar{x})$ of the source and dipole distributions, the perturbation velocity components (u_x, v_r, $v_{\theta a}$), pressure coefficient Cp, normal/side force co-efficients Cz, Cy and the moment coefficients C_{mz}, C_{my}.

Subsonic flows, at low mach No. past axi-symmetric slender bodies may be treated as incompressible and where Reynolds No. is near 2×10^6 or greater (Turbulent Boundary Layer) may be apprximated to inviscid flows [6] because the boundary layer is thin and not subject to separation. Therefore, axi-symmetric bodies at small angles of yaw or incidence (limited to 6°) may also be treated by this approach. Solution for such flows have been obtained by several authors by treating them as inviscid incompressible flows. The governing equation for the velocity potential ϕ for such flows is the well-known 'Laplace Equation'.

$$\nabla^2 \phi = 0$$

$$\phi_{xx} + \frac{1}{r} \phi_r + \phi_{rr} = 0 \qquad 2.1$$

The solution to the above Governing equation should further satisfy the boundary conditions as given here.

1. 'Flow Tangency' Conditions :- $\vec{V} . \vec{n} = 0$ on the body (2.2)

The flow on body surface is tangential and the velocity normal to surface is zero. Since $\vec{V} = \nabla\phi$ so $\vec{\nabla\phi}.\vec{n}=0$.

2. 'Remote Flow' conditions :- Perturbation velocity potential at infinity is zero

$$\phi = 0 \quad \text{at} \quad r = \infty \tag{2.3}$$

An axially symmetric body is represented by $r = r(x)$

$$r - r(x) = f(x,r) = 0$$

$$\vec{n} = \nabla f = \frac{-dr(x)}{dx} i + j$$

where i,j are unit vectors in x and r directions.

So $\vec{V} . \vec{n} = \vec{\nabla\phi}.\vec{n} = \left(U_\infty + u_x\right) x \frac{dr(x)}{dx} - v_r = 0$ (2.4)

Where u_x and v_r are the perturbation velocity components in x and r directions.

From 2.4 we can state

$$\frac{\text{Total radial vel.}}{\text{Total axial vel.}} = \text{slope of body.} \tag{2.4 (b)}$$

2.2 Isolated body solution

As indicated earlier in chapter 1, an isolated axi-symmetric body in uniform flow is represented by internal singularities distributed along the axis of the body.

The perturbation velocity potential $\phi = \frac{-1}{4\pi} \int_0^1 \frac{f(\bar{x})\, d\bar{x}}{\sqrt{R}}$ (2.5)

Where $f(\bar{x})$ is the source distribution function along the axis of body.

Without loss of generality the body length is taken as 1

$R = (\bar{x}-x)^2 + r^2$, the distance P D Ref. fig.(1)

P = Field point P (x,r,θ)

D = the position $(\bar{x},o)$ of linear element of singularity distribution

$\bar{x}$ = dummy variable, which represents location of singularity distribution.

The axial and radial perturbation velocity components at a field point P are obtained by differentiating ϕ along respective directions.

$$v_r = \frac{\partial \phi}{\partial r} = \frac{r}{4\pi} \int_0^1 \frac{f(\bar{x})\, d\bar{x}}{R^{3/2}} \qquad (2.6)$$

$$u_x = \frac{\partial \phi}{\partial x} = \frac{-1}{4\pi} \int_0^1 \frac{f(x)\,(\bar{x} - x)\, dx}{R^{3/2}} \qquad (2.7)$$

$$= x \int_0^1 \frac{f(\bar{x})\, d\bar{x}}{R^{3/2}} - \int_0^1 \frac{f(\bar{x})\, \bar{x}\, d\bar{x}}{R^{3/2}} \qquad (2.8)$$

2.3 Solution of polynomial source distribution $f(\bar{x})$

In order to represent the body accurately, a review of work of previous authors and their choice of $f(\bar{x})$ is essential. Accuracy and sensitivity of the method is dependent

upon proper choice of $f(\bar{x})$. Von Karman [2] used $f(\bar{x})$ constant over various segments along axis. Zedan [3] used linear variation of $f(\bar{x})$ and in a later work used parabolic variation of $f(x)$ over different segments. Christopher and Shaw [6] chose multiple polynomial, (3-polynomials of degree 10 each). Based on their experience, we have tried and chosen a single polynomial. A single polynomial of degree 8 is found to represent an axi-symmetric body fairly accurately

$$\text{So } f(\bar{x}) = C_o + C_1 \bar{x} + C_2 \bar{x}^2 \quad - - - - \quad C_n \bar{x}$$

$$= \sum_{o}^{n} C_j \bar{x}^j \tag{2.9}$$

Solution for $f(\bar{x})$ needs evaluation of the integral of form

$$I_j = \int_o^1 \frac{\bar{x}^j d\bar{x}}{R^{3/2}} \tag{2.10}$$

$$R = R(\bar{x}, x., r, \theta)$$

It is interesting to state here that I_j is easily determined from the table of integrals and it is not calculated by quadrature numerical integration. The expressions for the indefinite integrals of the form of I_j are given in recursive form in the book 'Table of integrals, Series and Products' by Gradshteyn and Ryzhik [9]. These are reproduced in App. A. C_j is evaluated by imposing the boundary conditions at n+1 control stations P on the body.

Substituting v_r , u_x in eqn. (2.4) viz.

$$v_t = \{U_\infty + u_x\} x \frac{dr(x)}{dx}$$

where $\frac{dr(x)}{dx}$ = slope of the body at field point P

Then eqn. (2.4) in vector form is

$$r_i \sum_{j=o}^{n} C_j \times I_j = U_\infty + x_i \sum_{j=o}^{n} C_j x I_j - \sum_{j=}^{n} C_j \times I_{j+1} \times \frac{dr(x)}{dx} \quad (2.11)$$

Taking $U_\infty = 1$, (2.11) gives (n+1) eqn. by moving field point P_i at n+1 control point of the form

$$AC = B$$

$$C = A^{-1}B$$

where C = unknown co-efficients C_j

A = Sq. matrix of order (n+1) = $A(i,j) = r_i x I_j - (x_i x I_j - I_{j+1}) x \frac{dr_i}{dx}$

$$B = B(i) = \frac{dr_i}{dx}$$

By solution of eqn. (2.11), we obtain (n+1) values of unknown variable C_j knowing C_j, the source distribution function $f(\bar{x})$, and the flow variables and the perturbation velocity components $v_r(i)$, $u_x(i)$ are readily computed.

2.4 Flow with interference

Consider two axi-symmetric bodies b_1 and b_2 laterally separated by a distance 'a' and axially placed in a uniform flow U_∞. (fig. 2).

Due to the presence of body b_2, the body b_1 is no longer placed in a uniform flow hence it may not be adequately represented by the source distribution along the axis. Similarly body b_2 cannot be adequately represented by a source distri-

bution along the axis. According to circle image theorem of Milne-Thompson [10], the source distribution have to be displaced off the axes towards each other as shown in fig.2(a) and 2(b). The lines on which sources are distributed may be called as image or delta lines. Martin [7] has given an expression for calculation of displacement distance δ, for a 2-dimensional case, for two identical bodies by making repeated applications of circle image theorem.

$$\delta = \frac{a}{2} \times \left\{1 - \sqrt{1 - \left(\frac{2r}{a}\right)^2}\right\} \qquad (2.12)$$

where δ, r are the displacement or delta distance, radius of circles C_1 and C_2 at any cross-section cc. From this equation it is clear that δ depends on geometry and not on strength of sources i.e. $\delta = \delta (r , a)$.

Martin [7] has solved the interference problem by distributing discrete distribution of dipoles i.e. sources of the dipole along delta line and the sinks along the axis of the body ref. fig. (2b). The discrete distribution of singularities gives pressure distribution which is in good agreement at control points but not at test points. Therefore, a continuous distribution of dipole $f_d(\bar{x})$ is tried and utilized to nullify the flow induced by the presence of the other body so that the resultant flow is tangential to body surface (the source distribution of dipole along the delta line and the sink distribution along the axis). The resulting flow is obtainable

by superposition of the flow due to source strength functions $f_1(\bar{x})$, $f_2(\bar{x})$ representing isolated bodies b_1 and b_2 uniform free stream U_∞ and that due to dipole functions $f_1 d(\bar{x})$, $f_2 d(\bar{x})$. The tangency boundary condition given by eqn. 2.4 is applicable for the total flow. i.e.

$$v_{rt} = (U_\infty + u_{xt}) \times \frac{dr(x)}{dx} \qquad (2.13)$$

where v_{rt}, , u_{xt} are the total or resulting radial and axial perturbation velocity components due to all singularities present in the flow.

$$\left.\begin{aligned} v_{rt} &= v_{s1} + v_{s2} + v_{d1} - v_{d2} \\ u_{xt} &= u_{s1} + u_{s2} + u_{d1} + u_{d2} \end{aligned}\right] \qquad (2.14)$$

where v and u represent radial and axial perturbation components of velocities subscript s,d, represent these components due to sources and dipoles. Substituting values of u_{xt} and v_{rt} from eqn. (2.14) in eqn. (2.13) we obtain another relation given as below

$$\frac{\Delta v_r}{\Delta u_x} = \frac{dr(x)}{dx} \qquad (2.15)$$

where Δv_r Δu_x , are increments in radial and axial induced velocities over and above those of single body in uniform flow.

It follows from eqn. (2.15) that the induced velocities due to additional singularities i.e. $f_2(\bar{x})$, $f_1 d(\bar{x})$, $f_2 d(\bar{x})$ also satisfy tangency condition on field point P., on the body b_1.

$$\Delta v_r = v_{s2} + v_{d1} - v_{d2}$$

$$\Delta u_x = u_{s2} + u_{d1} + u_{d2}$$

Expressions for v_{d1}, v_{d2}, u_{d1} and u_{d2} are given in eqn. (2.17) and (2.18).

2.5 Solution for the dipole strength function $f_d(\bar{x})$

The velocity potential ϕ_d due to a dipole distribution at a field point p(x, r, θ) is given as

$$\phi_d = \phi_{dp} + \phi_{dn}$$

$$= \frac{-1}{4\pi} \int_0^1 \frac{f_d(\bar{x})\, d\bar{x}}{\sqrt{R_\xi}} + \frac{1}{4\pi} \int_0^1 \frac{f_d(\bar{x})\, d\bar{x}}{\sqrt{R}} \qquad (2.16)$$

Where ϕ_{dp}, ϕ_{dn} are velocity potential due to source and sink respectively.

$$R_\xi = (\bar{x}-x)^2 + r_\delta^2 \qquad \text{Ref. fig. (3)}$$

$$R_\xi^2 = \xi^2 + r^2 - 2 r \xi \cos\theta$$

Let v_d = radial velocity due to dipole fn. $f_d(\bar{x})$ at P (x, r, θ)

$$= \frac{\partial \phi_d}{\partial r} = \frac{r\xi}{4\pi} \int_0^1 \frac{f_d(\bar{x})\, d\bar{x}}{R_\xi^{3/2}} - \frac{r}{4\pi} \int_0^1 \frac{f_d(\bar{x})\, d\bar{x}}{R^{3/2}} \qquad (2.17)$$

u_d = axial perturbation velocity due to dipole function $f_d(\bar{x})$ at P $(x., r, \theta)$

$$= \frac{\partial \phi_d}{\partial x} = -\frac{1}{4\pi} \int_0^1 \frac{f_d(\bar{x})\, (\bar{x}-x)\, d\bar{x}}{R_\xi^{3/2}} + \frac{1}{4\pi} \int_0^1 \frac{f_d(\bar{x})(\bar{x}-x)\, d\bar{x}}{R^{3/2}}$$

(2.18)

Substituting the value of v_d in equation (2.15) the solution for the (n+1) co-efficients of polynomial function $f_d(\bar{x})$ is obtained by moving field point $P(x, r, \theta)$ at (n+1) control points. The exact form of equation (2.15) in vector form are given in App. 'B' alongwith solution.

2.6 Determination of aerodynamic coefficients

Pressure distribution must be established first before finding other co-efficients like side force co-efficients C_y, loading $\frac{dc_y}{dx}$, moment coefficient C_{my}, C_{mz} etc.

$$Cp = 1 - \frac{V_n^2}{U_\infty^2}$$

V_n = Resultant velocity

$$V_n^2 = (U_\infty + u_x^2 + v_{rb}^2 + V_{\theta_a}^2)$$

u_{rt} = sum of perturbation velocity components in x direction

v_{rb} = sum of perturbation velocity components inradial direction.

$V_{\theta a}$ = perturbation velocity components tangential at Field Point P obtained by resolving v_r due to $f_2(\bar{x})$, $f_1 d(\bar{x})$, $f_2 d(\bar{x})$.

v_{rb} = $(U_\infty + u_x) \times \frac{d_r(x)}{dx}$ according to slender body theory and B.C.

v_{rb} = Approx. $\frac{dr(x)}{dx} \times U_\infty$ in case of u_x being small, which is the case when single slender body is placed in uniform stream. But u_x cannot be ignored in case of interfering flows in close proximity.

Knowing Cp other co-efficients are determined as discussed

below.

$$\frac{dc_y}{dx} = -\frac{r}{S_r} \int_0^{2\pi} Cp(\theta, x) \cos\theta \, d\theta \qquad (2.20)$$

Where S_r = ref. area = 2 x r (2.21)

$$\frac{dc_z}{dx} = -\frac{r}{S_r} \int_0^{2\pi} Cp(\theta, x) \sin\theta \, d\theta \qquad (2.22)$$

Then side force co-efficients

$$C_y = \int_0^1 \frac{dc_y}{dx} \, dx \qquad (2.23)$$

The normal force coefficient

$$C_z = \int_0^1 \frac{dc_z}{dx} \, dx \qquad (2.24)$$

Moment co-efficients

$$C_{m_Y} = \int_0^1 \frac{dc_y}{dx} (+x) \, dx \qquad (2.25)$$

$$C_{m_Y} = \int_0^1 \frac{dc_z}{dx} (-x) \, dx$$

All these co-efficients were determined by numerical integration by Simpsons rule dividing periphery in 24 intervals and the axial body in 10 intervals.

2.7 Presentation of results

The proposed method of representing the axially symmetric bodies by polynomial distribution of sources and dipoles, is applied to the study of flow over a family of sharp-ended bodies generated by arcs of parabola. This family of bodies is chosen in order to compare the results of the proposed method with the results of other authors who presented their results for similar bodies.

The variation of $\bar{\delta}$ as function of x and PR are plotted in fig. 9. The source and dipole strength functions $f(\bar{x})$ and $f_d(\bar{x})$ are plotted in fig. 10. The results of variation in error as function of x, θ, $\bar{\tau}$ and proximity (PR) are plotted in fig. 11, 12 and 13. The perturbation velocity components u_x, $V_{\theta a}$ are plotted in fig. 14,15 and 16. Pressure distribution (Cp) results are plotted in fig. 17. The side load distributions $\frac{dc_y}{dx}$ and side force co-effients C_y are plotted in fig. 18,19 and 20. Results of C_{mz} and C_{my} are not plotted as these values are just half of C_z and C_y for the family of bodies chosen i.e. symmetrical bodies about mid point.

CHAPTER 3

Lateral Flow

This chapter deals with the application of multipole singularities (MPS) for solving the lateral flow. When the onset flow is not axial, there will be a lateral component. This lateral flow may further be resolved into the yawing and incident flows, the yawing flow being the component along the line joining the centres of the bodies and the incident flow being normal to it. The system of two bodies may then be considered to be at an angle of yaw or at an angle of incidence or both. (Ref. fig. 5(b) and 6(b)).

We propose to determine the general flow over the axially symmetric body by application of slender body theory, treating each cross-section as 2-dimensional. This is valid for flows at an angle of incidence or yaw not exceeding 6° over slender bodies.

3.1 Interfering flows

Consider the flow as shown in fig. 5(a) and 5(b). If a single body C_1 was present in uniform stream V_∞, then a doublet of appropriate strength aligned in y-direction, the direction of onset flow, could have satisfied the boundary conditions. Then the solution was $V_{\theta 1} = -2 V_\infty \sin \theta$, $V_r = 0$ on body surface.

But the presence of body C_2 makes the onset flow V_∞ non-uniform. It is proposed to represent the circular body in non-uniform flow by a series of MPS placed at the centre of the circle. The stream function ψ_n of a MPS of order N is obtained by successive differentiation N times of stream function of a source ψ_s along a direction. The direction of differentiation may be called the direction of alignment of the MPS. The mathematical expressions for , $V_{\theta 1}$ and V_r induced by a MPS are given in the next section.

3.2 Stream function of multipole singularity

Consider a uniform onset flow V_∞ (Ref. fig. 7)
If a source of strength M_s is located at A (0,0), then stream function ψ_s at a field point P (r,θ) or P (y,z) due to the source at origin is

$$\psi_s = \frac{M_s}{2\pi} \tan^{-1} \left(\frac{z}{y}\right)$$

in polar co-ordinates

$$\psi_s = \frac{M_s}{2\pi} \theta \qquad 3.1$$

where $\theta = \tan^{-1} \left(\frac{z}{y}\right)$ $\qquad \frac{d\theta}{dy} = \frac{-z}{r^2} = \frac{-\sin\theta}{r}$

$$r = \sqrt{(y^2+z^2)}$$

denoting ψ_D, ψ_Q, ψ_o as ψ due to doublet, quadrupole and octopoles aligned in y direction by successive differentiation with reference to y direction we get.

$$\psi_D = \frac{-M_D}{2\pi r} \sin\theta ,$$

$$\psi_Q = \frac{M_Q}{2\pi r^2} \sin 2\theta$$

$$\psi_o = -2/\frac{M_O}{2\pi r^3} \sin 3\theta$$

So ψ_n = Stream function due to nth order differentiation, we have

$$\psi_n = \frac{(-1)^n (n-1)\,|}{2\pi r^n} M_n \sin n\theta \qquad (3.2)$$

If a series of MPS are placed at A(o,o) then stream function ψ_{mp} due to all these MPS upto order N at a field point P (r,θ) is given by the following relation

$$\psi_{mp} = \psi_D + \psi_Q + \psi_O + \cdots\cdots \psi_N$$

$$= \sum_{n=1}^{N} A_n M_n \frac{\sin n\theta}{r^n} \qquad (3.3)$$

where $A_n = \frac{(-1)^n \times (n-1)\,|}{2\pi}$,

Co-efficient A_n can be merged with strength M_n.

$$= \sum_{n=1}^{N} A_{m(n)} \frac{\sin n\theta}{r^n} \quad \text{where } A_{m(n)} = A_n \times M_n.$$

It may be observed from the above eqn. (3.3) that ψ_{mp} i.e. due to series of nth order MPS, aligned in y direction is sum of all sine terms of a Fourier series in θ. This implies that ψ_{mp} is anti-symmetric about y axis.

3.3 Yawing flow

The solution to the problem of lateral flow (yawing or incident) over the circles C_1 and C_2 is attempted by representing each circle C_1 and C_2 by a series of multipoles of different order say, upto N, aligned along the direction of flow (yaw or incident) and placed at the centres of circles. The strength of 2N MPS are determined by imposing the boundary conditions ψ=const. at N control points on each circle. An alternate way of imposing boundary condition is V_r=0 at N control points on each circles.

From the boundary conditions the total stream function, due to onset flow and both the MPS at the centres of circles C_1 and C_2, must be zero. Then resulting equation :

$$\text{on body } C_1 \quad \psi_{11} + \psi_{12} + \psi_{1\,\text{onset}} = 0$$

$$\text{on body } C_2 \quad \psi_{21} + \psi_{22} + \psi_{2\,\text{onset}} = 0 \qquad (3.4)$$

where 1st subscript of denotes the field point location and 2nd subscript denotes the location of MPS on circle C_1 or C_2 causing the stream function.

We also observe that

$$\psi_{1\,\text{onset}} = V_\infty r_1 \sin\theta_1$$
$$\psi_{2\,\text{onset}} = V_\infty r_2 \sin\theta_2 \qquad (3.5)$$

ψ_{11}, ψ_{12}, ψ_{22} and ψ_{21} are calculated as per eqn. (3.3)

$$\psi_{11} = \sum_{n=1}^{N} A_{m(n)} \frac{\sin n\theta_1}{r_1^n}$$

$$\psi_{12} = \sum_{n=1}^{N} A_{1(n)} \frac{\sin n\phi_1}{r_{b1}^n} \qquad (3.6)$$

likewise relations of ψ_{22} and ψ_{21} are calculated for field point P (r,θ) on circle C_2. By substituting expressions for ψ_{11}, ψ_{12} and $\psi_{1\ onset}$ from 3.5, 3.6 in eqn. 3.4 we obtain the resulting equation involving 2N unknowns. We therefore solve for these 2N unknowns $A_{m(n)}$, $A_{1(n)}$ by imposing boundary conditions at 2N control points (The resulting linear algebraic equation are solved by matrix inversion).

3.4 Mathematical relations for $V_{\theta 1}$, V_{r1}

Referring to figure 5(b)

$$V_{r1} = \frac{1}{r_1}\left[\frac{\partial\psi_{11}}{\partial\theta_1} + \frac{\partial\psi_{12}}{\partial\theta_1}\right] + \frac{1}{r_1}\frac{\partial\psi_{1\ onset}}{\partial\theta_1} \qquad (3.7)$$

$$\frac{\partial\psi_{12}}{\partial\theta_1} = \frac{\partial\psi_{12}}{\partial\phi_1} \times \frac{d\phi_1}{d\theta_1} + \frac{\partial\psi_{12}}{\partial r_{b1}} \times \frac{dr_{b1}}{d\theta_1} \qquad (3.8)$$

finally

$$V_{r1} = \frac{1}{r_1}\left[\sum_{n=1}^{n} \frac{nxA_{m(n)}}{r_1^n} \times \cos n\theta_1 + \sum_{n=1}^{n} \frac{nxA_{1(n)}}{r_{b1}^n} \cos n\phi_1 \times \frac{d\phi_1}{d\theta_1} - \sum_{n=1}^{n} \frac{nxA_{1(n)} \sin n\phi_1}{r_{b1}^{n+1}} \times \frac{dr_{b1}}{d\theta_1}\right] + \cos\theta_1 \qquad (3.9)$$

$$V_{O11} = -\frac{\partial \psi_{Total}}{\partial r_1} = -\left[\frac{\partial \psi_{11}}{\partial r_1} + \frac{\partial \psi_{12}}{\partial r_1} + \sin \theta_1\right]$$

$$= \sum_{n=1}^{n} \frac{nxA_{m(n)} \sin n\theta_1}{r_1^{n+1}} + \sum_{n=1}^{n} \frac{nxA_{1(n)} \sin n\phi_1}{r_{b1}^{n+1}} \times \frac{dr_{b1}}{dr_1}$$

$$- \sum_{n=1}^{n} \frac{nxA_{1(n)} \cos n\phi_1}{r_{b1}^{n+1}} \times \frac{d\phi_1}{dr_1} - \sin \theta_1 \qquad (3.10)$$

Similar relations are obtained for $V_{\theta 12}$ and V_{r2}.

3.5 Incident flow

When flow is at an angle of attack α to the axial direction, the resolved component along z direction is W_∞ (fig.6b refers). The MPS are aligned along z direction. θ is measured with reference to z direction onset is given by eqn. 3.11.

$$\psi_1 \text{onset} = -W_\infty r_1 \sin \theta_1 \qquad P \text{ on } C1$$
$$\psi_2 \text{onset} = W_\infty (a - r_2 \cdot \sin \theta_2) \qquad P \text{ on } C2 \qquad (3.11)$$

$W_\infty = U_\infty \sin\alpha = U_\infty \times \alpha$, Taking $U_\infty = 1$, max=.1 radian,

$W_\infty = .10$ (max.)

The relations (3.4), (3.5), (3.9) and (3.10) remain unchanged.

Since geometry of incident flow is different than that of yawing flow, only geometric relations between θ, ϕ, r_{a1} differ. By substituting proper values of $\frac{d\phi_1}{d\theta_1}$, $\frac{dr_{a1}}{dr_1}$ in relation (3.9) and (3.10) V_{r1} and $V_{\theta 11}$ are calculated.

3.6 Combined solution of axial and lateral flows

After finding out the perturbation velocity components like u_x, v_r and $V_{\theta a}$ from the axial solution and $V_{\theta l}$ and V_r from the lateral solution, the resultant velocity V_n is easily calculated by adding the various velocity components in vector form. The pressure coefficient Cp (θ,x) side force gradients $\frac{dc_y}{dx}$, $\frac{dc_z}{dx}$, side force co-efficients C_y, C_z and moment coefficients C_{my}, C_{mz} are calculated as follows.

$$\bar{V_n} = (U_\infty + u_x)\, i + v_r\, j + V_\theta\, k$$

where u_x, v_r, V_θ are axial, radial and tangential velocity components (Ref. fig. 8) of the combined solution such that

$$V_\theta = V_{\theta a} + V_{\theta l},\quad v_r = v_{rb} + V_r$$

$$V_n = \sqrt{(U_\infty + u_x)^2 + v_r^2 + V_\theta^2}$$

$$Cp\ (\theta,x) = 1 - \frac{V_n^2}{U_\infty^2} \qquad \text{Taking } U_\infty = 1$$

$$= -\,(2\,u_x + v_r^2 + V_\theta^2 + u_x^2) \qquad (3.12)$$

$$\text{Side force loading } \frac{dc_y}{dx} = -\frac{1}{S_r}\int_0^{2\pi} r\, Cp \cos\theta\, d\theta \qquad (3.13)$$

$$\text{Normal force loading } \frac{dc_z}{dx} = -\frac{1}{S_r}\int_0^{2\pi} Cp \sin\theta \times r\, d\theta \qquad (3.14)$$

S_r = ref. cross-sectional area = $2x\pi \times 1$

Side force co-efficiency $C_y = \int (\frac{dc_y}{dx})\, dx$ (3.15)

Normal force co-efficient $C_z = \int (\frac{dc_z}{dx})\, dx$ (3.16)

Moment co-efficients (about nose) $C_{m_z} = \int_0^1 (+x)\, (\frac{dc_y}{dx})\, dx$ (3.17)

$$C_{m_y} = \int_0^1 (-x)\, (\frac{dc_z}{dx})\, dx \quad (3.18)$$

Analytical solutions of equations 3.13 to 3.18 are difficult, so their solutions have been obtained by numerical computations by Simpson's Rule.

3.7 Presentation of results

Results of $V_{\theta 1}$ and V_r in yawing flow over two identical and different circles are presented in fig. 21, 22 and 23. Results of $V_{\theta 1}$ and V_r as function of θ in incident flow are presented in fig. 24. The side load and normal loads of yawing and incident flow are presented with the results of axial flow in fig. 25. Normal load distribution for incident flow are presented in fig. 26.

CHAPTER 4

Discussion of results and conclusions

In this chapter the results obtained by the present method of representing axially symmetric bodies are reviewed and compared with those obtained by other methods and by other authors. The error in representing the body with and without interference has been compared along with distribution of pressure and side forces. The factors on which the sensitivity and accuracy of 3-dimensional dipole method depends namely, calculation of delta-line, choice of form of source and dipole distribution and the degree of polynomial are discussed; relative significance of lateral flow studied. Finally, the suitability of the present method assessed.

4.1 Comparative study of results

As stated in chapter 2, the proposed method of representing the axially symmetric bodies by polynomial distribution of sources and other dipoles, is applied to the study of flow over a family of sharp-ended bodies generated by arcs of parabola. According to flow tangency condition the normal velocity should be zero at all points on the surface of the body. This condition is exactly satisfied at chosen control points but at other points, this condition in general is not exactly satisfied. The normal velocity (V_{norm}) at test points chosen midway between the control points called the leakage velocity, is a measure of error associated with the

method. V_{norm} normalised with respect to thickness ratio has been presented as error in figs. No. 11 to 13. It may be seen that the maximum error i.e. 4.9% corresponding to τ_1=.20, τ_2= .20 and PR = 1.1, θ=180° is comparable with the maximum error associated with SDQ model of Christopher and Shaw (4.9%). The SDQO model of Christopher and Shaw gives slightly less error i.e. 4.0%.

It is worthwhile to state that all the error results are plotted for θ=180° because error at θ=180° is found to be maximum. Since boundary conditions, for obtaining the solution, were imposed at θ=0°, where the error was found to be less than 1% at all points on checking. The variation in perturbation velocity components u_x, $V_{\theta a}$ has been presented in fig. 14 to 16 as function of x, PR, and θ. Results for comparison are not available. However, our observations are as follows

(a) u_x rises towards - U_∞ steeply between x=.05 to x=.00 because at x=0, there is a stagnation point where total velocity is zero i.e. $U_\infty+u_x=0$. So $u_x= -U_\infty$. This trend is clearly exhibited by the results.

(b) u_x appears to be proportional to τ for small values of τ but rises faster for high τ.

(c) There is continuous accceleration of flow from nose to the midele and deceleration from the middle to tail.

(d) The variation in ux is maximum along meridian plane ($\theta=0$) but there is no change in u_x due to interference at $\theta=180^\circ$. It shows that interference effects increase from $\theta=180^\circ$ to $\theta=0$ from minimum to maximum.

(e) u_x approaches ∞ in case of touching bodies at x=.50 as may be expected.

Pressure distribution results are plotted in fig. 17 as function of x, θ at PR=1.1 . Our observations are as follows.

(a) Cp variation is maximum near middle portion of the body along $\theta=0$. The figures show that suction is created and attractive loads are acting on interfering bodies in the axial flow.

(b) Interference effects are less near nose of bodies (Cp values for isolated and interferring cases are close) because of larger local proximity.

(c) Cp values at $\theta=180^\circ$ are same for interfering as well isolated body. (No interference at $\theta=180^\circ$).

(d) Cp values are finite near nose.

(e) Larger loads are created as τ increases.

Side force loading $\frac{dc_y}{dx}$ results for axial, yawing and incident flows are presented in fig. 18 to 19 These results are compared with the results obtained by panel

method and those by Christopher and Shaw. It may be seen that the results of present study agree with the results obtained by 'panel method' and 'Christopher and Shaw' better in close proximity near middle portions of the bodies. Our results predicted near (x=.10 to .35) slightly over-estimate the side force gradients. The results of normal loading $\frac{dc_z}{dx}$ for a combined axial and incident flow corresponding to α=.10 radian, are plotted in fig. 26. It may be seen that in the range x=.2 to .35 our results overestimate $\frac{dc_z}{dx}$ as compared to the results of panel method and Christopher and Shaw. But the results are comparable near nose, tail and middle portions of the bodies. Results of perturbation velocity components $V_{\theta 1}$ and V_r of the lateral flow are presented in fig. 21 to 24. Results of lateral flow are not available separately for comparison; however, our observations are as follows

(a) Yawing flow produces repulsive forces in the bodies but incident flow produces attractive forces as the axial flow does.

(b) The flow in general is retarded in yawing case whereas the incident flow is accelerated.

(c) V_r (V_{norm}) as stated earlier is a measure of error. The values of V_{norm} are large in incident and yawing flow.

At PR=1.1, identical bodies

$V_{norm} = 20 \times 10^{-2}$ incident flow

$V_{norm} = 15 \times 10^{-2}$ yawing flow

These values are with reference to onset lateral flow i.e. W_∞ and V_∞. Even though, the errors are large with reference to lateral flow but these errors are small and of the same order as the axial flow when compared with U_∞ i.e. $V_{norm}=2\times10^{-2}$, 1.5×10^{-2} for incident and yawing flow as compared to U_∞. The contribution of lateral flow is very small because angles of incidence and yaw are small (limited to .10 radian) as dictated by slender body theory. Side force co-efficient (C_y) obtained by integration of the gradient $\frac{dc_y}{dx}$ results are presented as function of PR and $\bar{\sigma}$ in fig. 20.

This suggests that

One can make a choice between the load encountered at a particular proximity if external stores in these proximities are to be carried. It is seen that the side force co-efficient steadily increases with proximity and $\bar{\sigma}$ until PR=1.5. The value of C_y rises steeply between PR=1.5 to 1.

4.2 Sensitivity, improvement and application of the method

The accuracy of the method depends on accurate determination of delta line by taking 3D-approach, choice of polynomial functions $f(\bar{x})$, $fd(\bar{x})$ and the degree of polynomial. In the

present study delta line calculations are based on 2D approach. This needs improvement for greater accuracy. Regarding proper choice of $f(\bar{x})$ and $f_d(\bar{x})$ we have taken into consideration the experience of other authors and consequently we could represent body (isolated case and with interference) by a polynomial of degrees 8 for the profile chosen. It must be mentioned here that a polynomial of higher degrees than 8 did not improve accuracy; rather polynomials of degrees greater than 10 led to ill-conditioning of matrices.

This method is applicable to sharp nosed bodies but it can be tried with blunt nosed bodies by redistribution of polynomial functions between x=.02 to .98 or so. This method has been tried on identical, symmetric, parabolic bodies with varying τ, between 0.10 to 0.40 (=10, 20, 40%) and for different proximities. The body profile being represented by $r(x)=2\tau(x-x^2)$, where τ=thickness ratio (d/l). The method gives good results for interference between bodies of unequal thickness ratios (τ) also. The method is easily and readily extendable to non-identical bodies laterally separated, staggered and with modifications to skewed bodies too. Our further suggestions for extension and application of the method are as follows.

1. Interference between axi-symmetric bodies in compressible subsonic and supersonic flows.
2. Interference between cluster of axi-symmetric bodies.

4.3 Conclusions

Following conclusions are drawn from the present study.

(a) Discrete distribution of singularities

Representing an axi-symmetric body by discrete distributions as large as 35 failed because of large leakage velocities at test points. This method was given up after initial trials.

(b) This study suggests a fairly accurate method of rapid determination of interference effects between axially symmetric bodies. This may supplement more accurate panel methods by providing an approximate initial solution over which panel methods may be efficiently used to improve accuracy.

References

1. Rankine, W.J.M., 'On the mathematical theory of streamlines, especially those with four foci and upwards, Phil. Trans. 161, 267, 1871.

2. VON-Karman, T. 'Calculation of pressure distribution on airship , NACA, TM 574, 1930.

3. James, R.M. 'A general analytical method for axi-symmetric incompressible potential flow about bodies of revolution. Computer methods in applied mechanics and engg. 12, 1977, pp. 47-67.

4. Zedan and Dalton, 'Higher order singularities distribution for potential flow about bodies of revolution. Computer methods in applied mechanics and engg. 21, 1980, pp.295-314.

5. Campbell, 'Calculation of potential flow past axi-symmetric bodies using axial sources and least square method. J. Aircraft Jun 84.

6. Christopher, P.A.T. and Shaw, C.T. 'Generation of axi-symmetric body shapes in subsonic flow by means of polynomial distribution of sources and doublets along the axis of symmetry', A. Memo 8110, Oct. 1981.

7. Marin, Smith Saunders, 'Image system solution for store aerodynamics with interference Part 1', J.Aircraft, 12, 3 March, 1975.

8. Christopher, P.A.T. and Shaw, C.T. 'The use of multipoles for calculating aerodynamic interference between bodies of revolution in subsonic flow', A. Memo 8301, Feb. 1983.

9. 'Table of Integrals, series and Products' by Gradshteyn and Ryzhik.

10. Milne, thompson, 'Theoretical Hydrodynamics'

11. Karamcheti, K. 'Principles of ideal fluid Aerodynamics'.

12. Johnson, F.T. 'A general panel method for the analysis and design of arbitrary configurations in incompressible flows. NASA CR 3079, May 1980.

Appendix (A)

Evaluation of integrals $\int \frac{\bar{x}^m d\bar{x}}{R^{3/2}}$

$$I_m = \int \frac{\bar{x}^m d\bar{x}}{R^{3/2}} = \frac{\bar{x}^{m-1}}{(m-2)\sqrt{R}} + \frac{(2m-3)x}{(m-2)} * \int \frac{\bar{x}^{m-1} d\bar{x}}{R^{3/2}} - \frac{(m-1)(x^2+r^2)}{(m-2)} * \int \frac{\bar{x}^{m-2} d\bar{x}}{R^{3/2}}$$

At m=2 where $R=(\bar{x}-x)^2+r^2$

$$I_2 = \frac{-\bar{x}}{\sqrt{R}} + x \int \frac{\bar{x}}{R^{3/2}} d\bar{x} + \int \frac{d\bar{x}}{\sqrt{R}}$$

$$= \frac{\bar{x}}{\sqrt{R}} + x * I_1 + I_o$$

$$\int \frac{d\bar{x}}{R^{3/2}} = \frac{(\bar{x}-x)}{\sqrt{R}}$$

$$I_o = \int \frac{d\bar{x}}{\sqrt{R}} = \text{Arsh} \frac{(\bar{x}-x)}{r}$$

$$I_1 = \int \frac{\bar{x} d\bar{x}}{R^{3/2}}$$

Appendix (B)

Solution of the co-efficients of the polynomial distribution functions

From flow tangency condition we have

$$\frac{\Delta v_r}{\Delta u_x} = \frac{dr(x)}{dx} \qquad (2.15)$$

where $\Delta v_r = v_{s2} + v_{d1} - v_{a2}$

$$\Delta u_x = u_{s2} + u_{d1} + u_{d2}$$

v_{s2} and u_{s2} are the induced velocities (radial, axial) by the presence of body b_2 in the flow represented by a function $f_2(\bar{x})$. Function $f_2(\bar{x})$ is calculated similar to the method given in para 2.3 (eqn. 2.11). So v_{s2} and u_{s2} are known parameters. Substituting for v_r and u_x in eqn (2.15) we obtain a relation

$$(u_{d1}+u_{d2}) \frac{dr(x)}{dx} - (v_{d1} - u_{d2}) = v_{s2} - u_{s2} \times \frac{dr(x)}{dx} \qquad (2.26)$$

Putting u_{d1}, u_{d2}, v_{d1}, v_{d2} in terms of $f_{1d}(\bar{x})$, $f_{2d}(\bar{x})$ etc. as given in eqn. 2.17 and 2.18

$$v_{d1} = r_{d11} \int_0^1 \frac{f_{1d}(\bar{x})\, d\bar{x}}{R_\delta^{3/2}} - r_1 \int_0^1 \frac{f_{1d}(\bar{x})\, d\bar{x}}{R^{3/2}} \qquad (2.27)$$

where $R_\delta = (\bar{x}-x)^2 + r_{d11}^2$ Ref. fig. 4

$$v_{d1} = \left\{ r_{d11} \times \sum_{j=o}^{n} I_{d(j)} - r_1 \times \sum_{j=o}^{n} I_{d(j)} \right\} \times C_{d(j)} \qquad (2.28)$$

By moving the field point P at (n+1) control points we obtain (n+1) eqns. and 2.28 is modified as follows in vector form.

$$v_{dl}(j) = \left\{ r_{dll}(i) \times Ad\,(i,j) \times \cos(\Theta_B - \Theta) - AA(i,j) \times r_1(i) \right\} \times C_{D(j)} \qquad (2.29)$$

By resolving velocities in radial direction along Θ.

Similarly

$$v_{d2(i)} = \left\{ r_{dl2(i)} \times B_{d(i,j)} \times \cos(\phi_B - \Theta) - BB(i,j) \times r_{bl(i)} \times \cos(\phi_1 - \Theta) \right\} \times Cd(j) \qquad (2.30)$$

where $Ad(i,j) = \sum_{j=o}^{n} I_{d(j)}$, $I_{b(j)} = \int_o^1 \frac{\bar{x}^j \, d\bar{x}}{R_b^{3/2}}$

$$Bd(i,j) = \sum_{j=o}^{n} I_{bd(j)} \quad , \quad I_{bd(j)} = \int_o^1 \frac{\bar{x}^j \, d\bar{x}}{R_{bd}^{3/2}}$$

$$BB(i,j) = \sum_{j=o}^{n} I_{b(j)} \quad , \quad R_b = (\bar{x} - x_i)^2 + r_{bl\,(i)}^2$$

$$AA(i,j) = \sum_{j=o}^{n} I(j) \qquad R_{bd} = (\bar{x} - x_i)^2 + r_{dl2(i)}^2$$

Further substitution gives us.

$$vd_1\,(i) = VV_1(i,j) \times cd(j) \qquad (2.31)$$

$$vd_2\,(i) = VV_2(i,j) \times cd(j)$$

where $VV_1(i,j) = r_{dll(i)} \times Ad\,(i,j) \times \cos(\Theta B - \Theta) - AA(i,j) \times r_1(i)$

$$VV_2(i,j) = r_{dl2(i)} \times Bd(i,j) \times \cos(\phi_B - \Theta) - BB(i,j) \times rb_1(i) \times \cos(\phi_1 - \Theta)$$

Similarly $ud_1(i) = \int_o^1 \frac{f_{1d}(\bar{x})(x_i - \bar{x})}{R^{3/2}} d\bar{x} - \int_o^1 \frac{f_{1d}(\bar{x})(x_i - \bar{x})}{R^{3/2}} d\bar{x}$

$$= x_i \sum_{j=o}^{n} Id(j) - \sum_{j=o}^{n} Id(j+1) - \left(x_i \sum_{j=o}^{n} I_j - \sum_{j=o}^{n} I(j+1) \right) \quad (2.32)$$

which in Matrix Form is

$$ud_1(i) = \left[\{x_i \, xAD)i,j) - Ad(i,j+1)\} - \{x_i \, xAA(i,j) - AA(i,j+1)\} \right] \text{xcd}(j)$$

$$ud_2(i) = \left[\{x_i \, xBd(i,j) - Bd(i,j+1)\} - \{x_i \, xBB(i,j) - BB(i,j+1)\} \right] \text{xcd}(j) \quad (2.33)$$

on substitution.

$$\left.\begin{aligned} ud_1(i) &= UU_1(i,j) \times cd(j) \\ ud_2(i) &= UU_2(i,j) \times cd(j) \end{aligned}\right] \quad (2.34)$$

where $UU_1(i,j) = \{x_i \times Ad(i,j) - Ad(i,j+1)\} - \{x_i \, xAA(i,j) - AA(i,j+1)\}$

$$UU_2(i,j) = \{x_i \times Bd(i,j) - Bd(i,j+1)\} - \{x_i \, BB(i,j) - BB(i,j+1)\} \quad (2.35)$$

Eqn. (2.41) can be put in matrix form as

$$\left[\{UU_1(i,j) + UU_2(i,j)\} \times \frac{dr_i}{dx} - \{VV_1(i,j) - VV_2(i,j)\} \right] \times cd(j)$$

$$= v_{s2}(i) - u_{s2}(i) \times \frac{dr_i}{dx} \quad (2.36)$$

which is of the form

$$FX = B$$

$$X = F^{-1} B$$

where $B = B(i)$ = R.H.S. of (2.36)

$X = X(j) = Cd(j)$ unknown. (2.37)

$$F = F(i,j) = \{UU_1(i,j) + UU_2(i,j)\} \times \frac{dr_i}{dx} - \{VV_1(i,j) - VV_2(i,j)\} \quad (2.38)$$

Appendix 'C'

Geometric Relations in Lateral Flow

Yawing Flow : (Ref. fig. 5b)

The main relation from which other derivatives and eqns. are drawn.

$$r_1 \sin \Theta_1 = R_{b1} \times \sin (\pi - \phi_1)$$

$$\frac{dR_{b1}}{d\Theta_1} = \frac{a \times r_1 \times \sin \Theta_1}{R_{b1}}$$

$$\frac{dR_{b1}}{dr_1} = \frac{r_1 - a \cos \Theta_1}{R_{b1}}$$

$$\frac{d\phi_1}{d\Theta_1} = \frac{1}{R_{b1} \times \cos \phi_1} \left\{ r_1 \cos \Theta_1 - \frac{dR_{b1}}{d\Theta_1} \sin \phi_1 \right\}$$

$$\frac{d\phi_1}{dr_1} = \frac{\sin \Theta_1}{R_{b1} \times \cos \phi_1} \left\{ 1 - \frac{dR_{b1}}{dr_1} \times \sin \phi_1 \right\}$$

Incident flow : (Ref. fig. 6b)

$$\frac{dR_{A1}}{d\Theta_1} = \frac{a\, r_1 \cos \Theta_1}{R_{A1}}$$

$$\frac{dR_{A1}}{dr_1} = \frac{r_1 + a \sin \Theta_1}{R_{A1}}$$

$$\frac{d\phi_1}{d\Theta_1} = \frac{1}{R_{A1} \times \sin \phi_1} \left\{ r_1 \sin \Theta_1 + \frac{dR_{A1}}{d\Theta_1} \times \cos \phi_1 \right\}$$

$$\frac{d\phi_1}{dr_1} = \frac{1}{R_{A1} \times \sin \phi_1} \left\{ \cos \phi_1 \times \frac{dR_{A1}}{dr_1} - \cos \Theta_1 \right\}$$

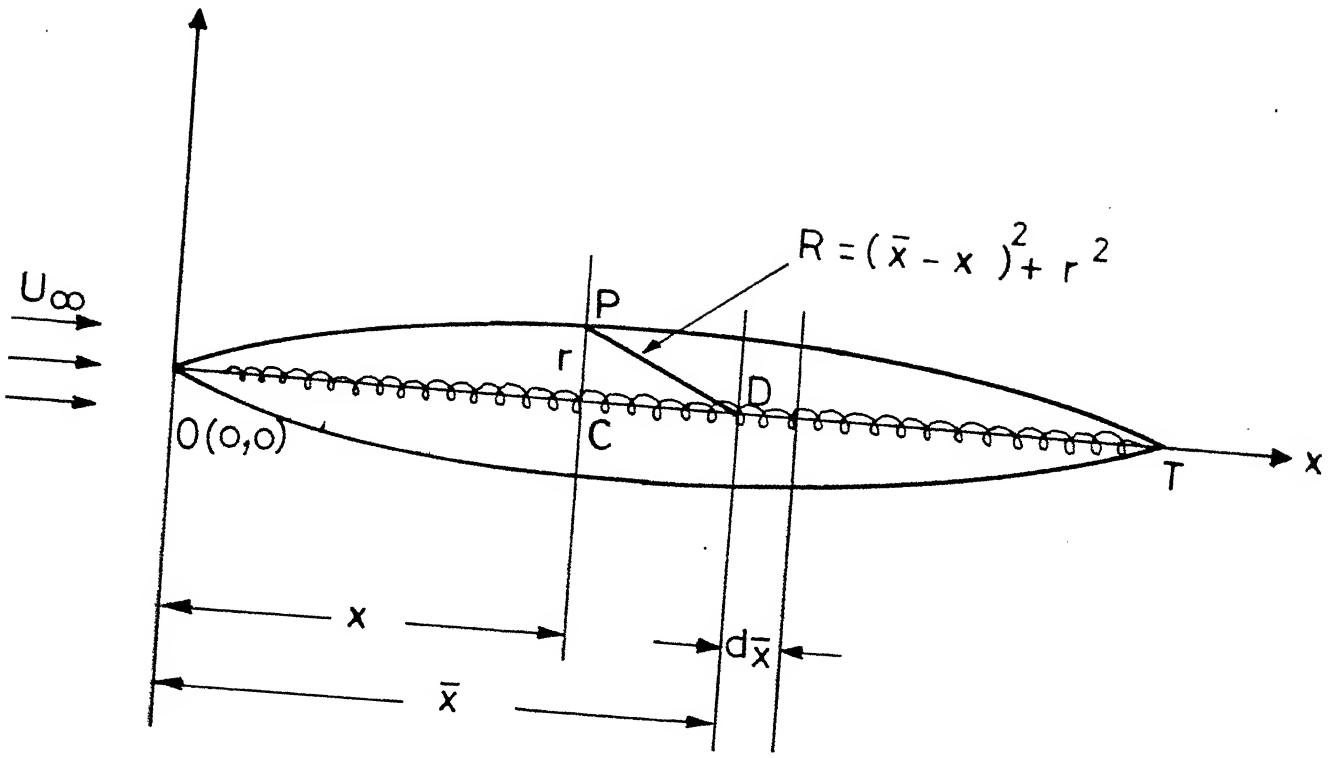

Fig.1 Isolated body in free stream

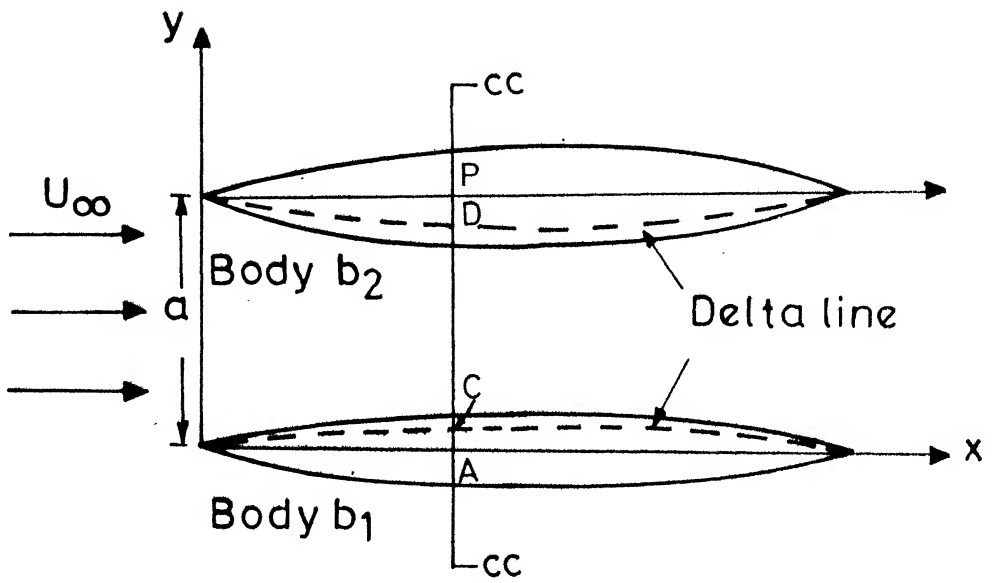

(a)

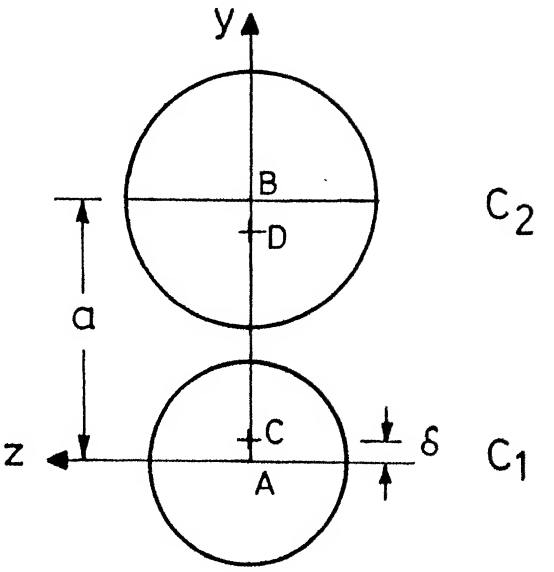

Cross section cc-cc

(b)

Fig.2 Interfering flows

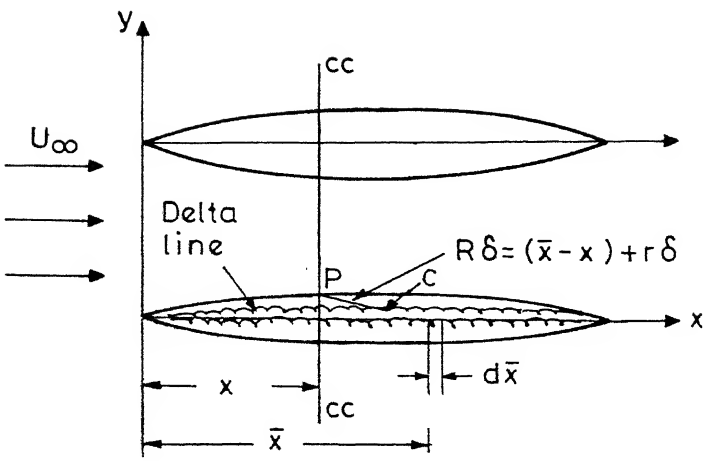

(a)

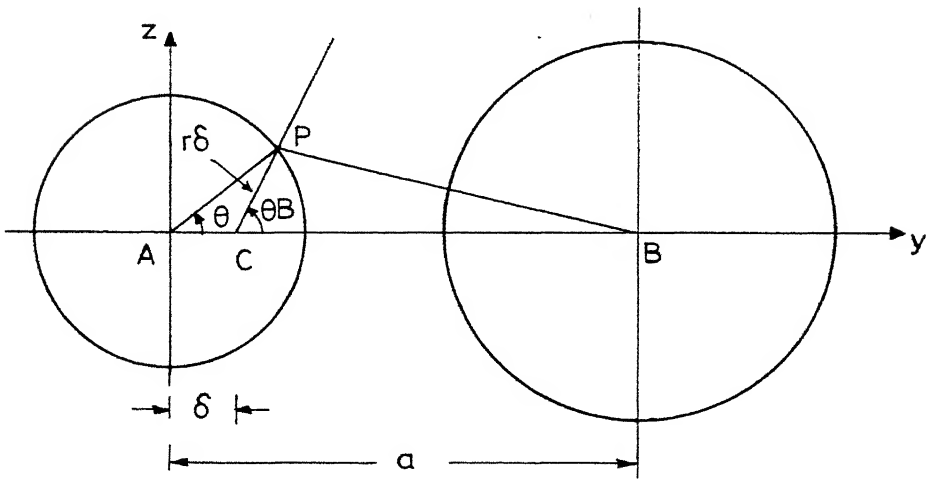

Cross section cc-cc (enlarged view)

(b)

Fig.3 Source and dipole flow model

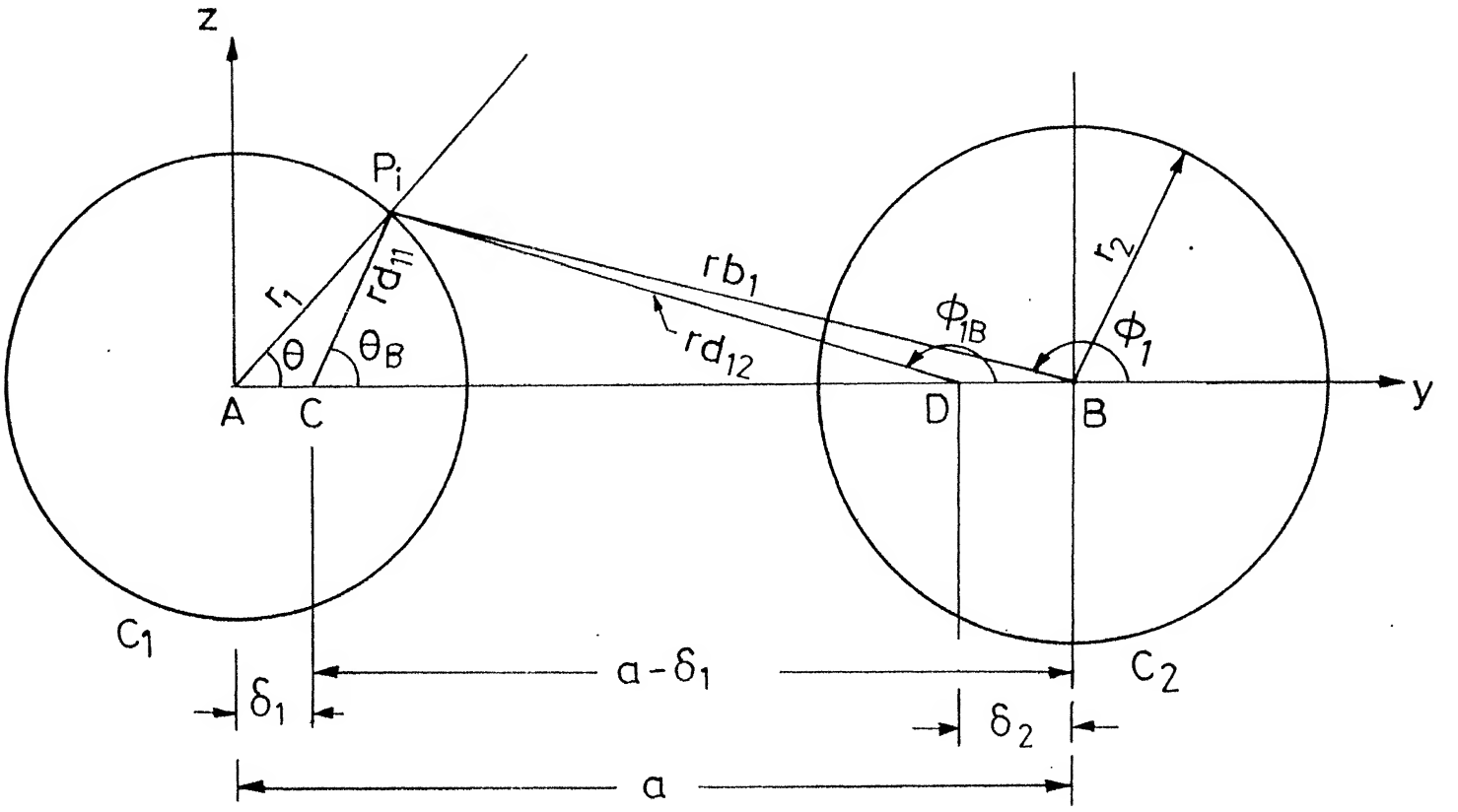

Cross-section of Fig. 3a
y-z plane

Fig. 4

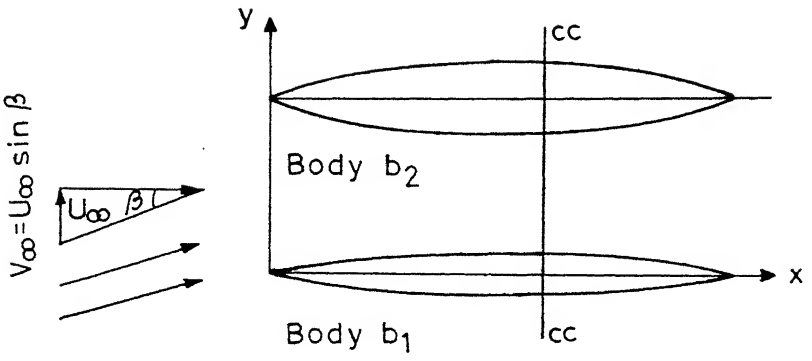

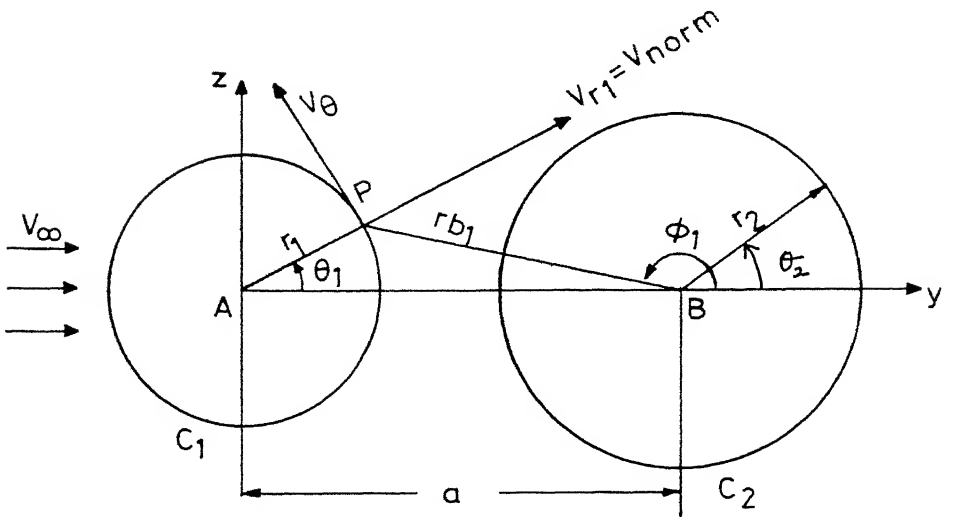

Cross section cc-cc

Fig.5 Axial flow at yaw

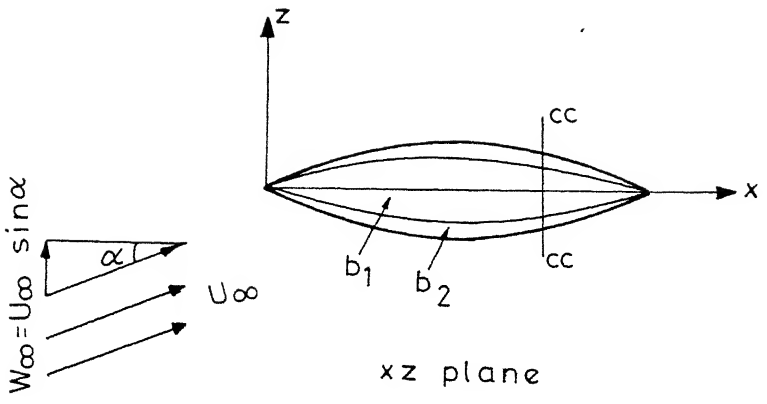

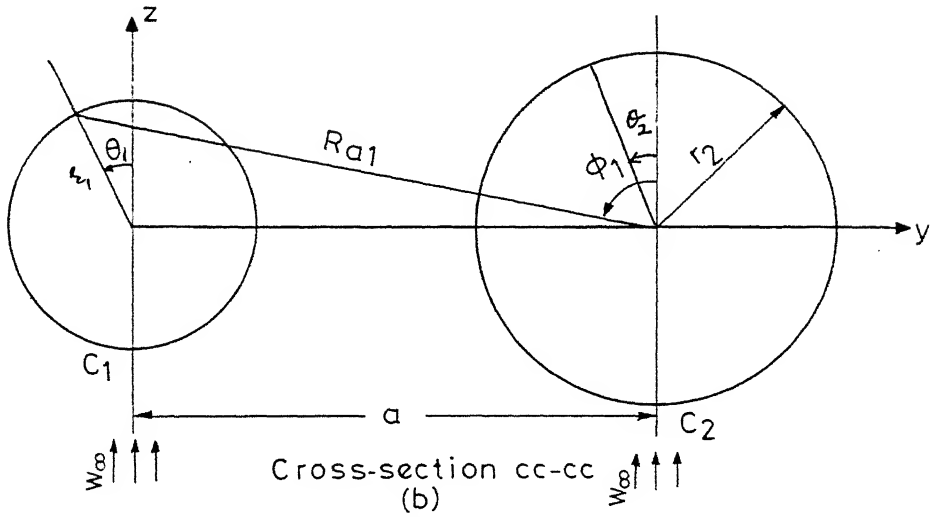

Fig.6 Axial flow at incidence

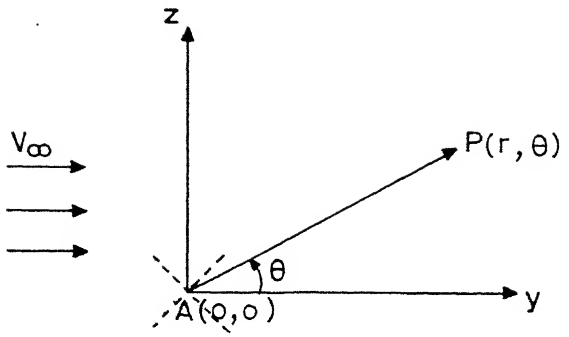

Fig. 7 Source and multipole singularity

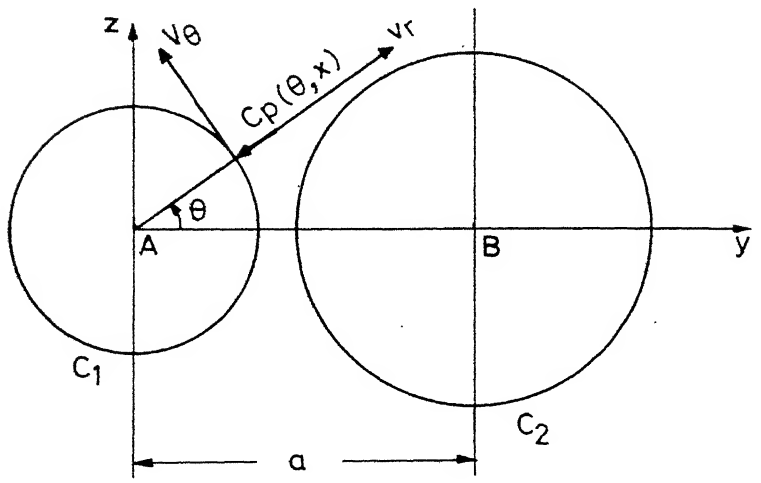

Fig. 8 Pressure distribution: combined flows

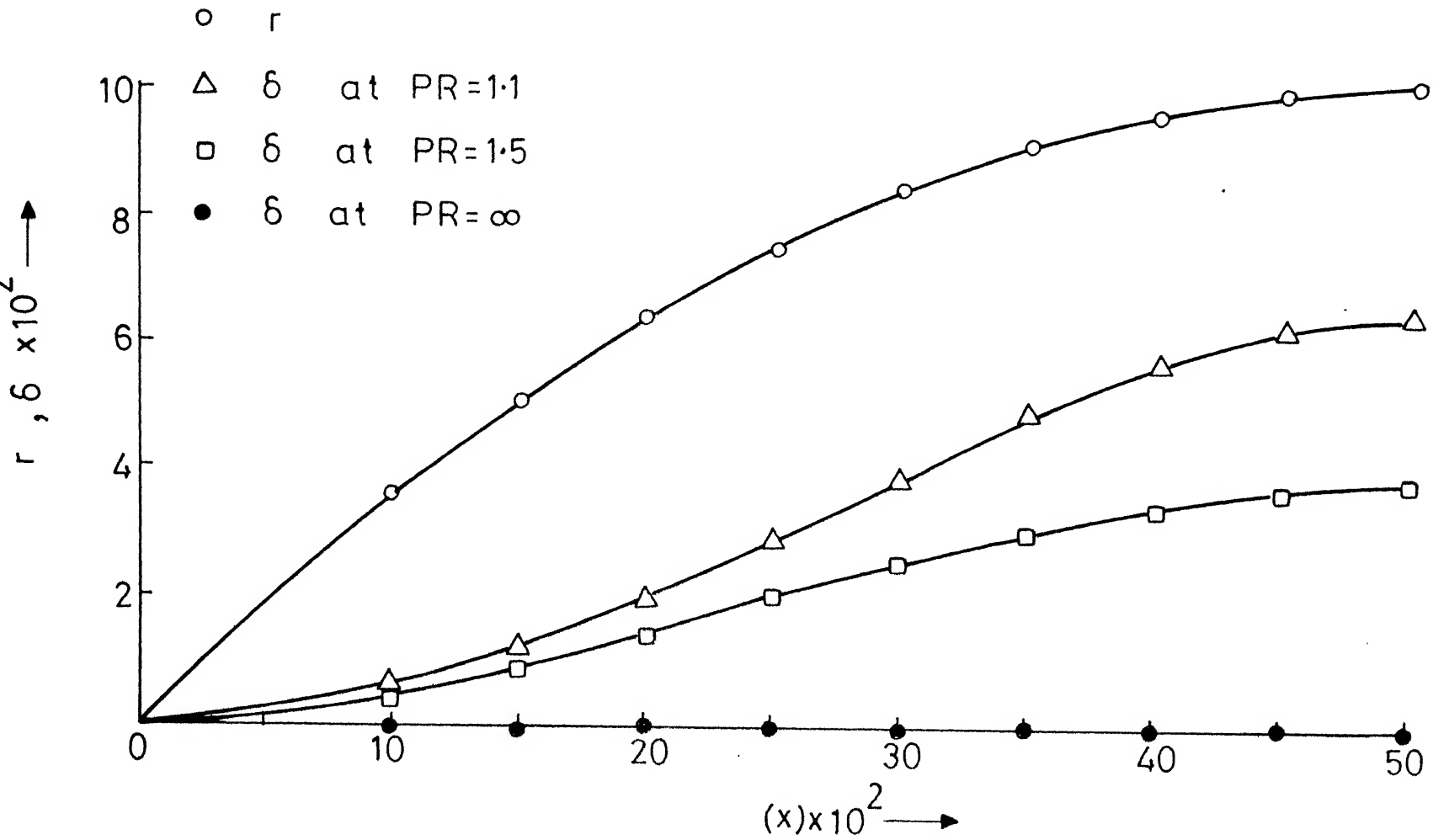

Fig.9 Displacement of delta line from axis
$\tau = \cdot 20$

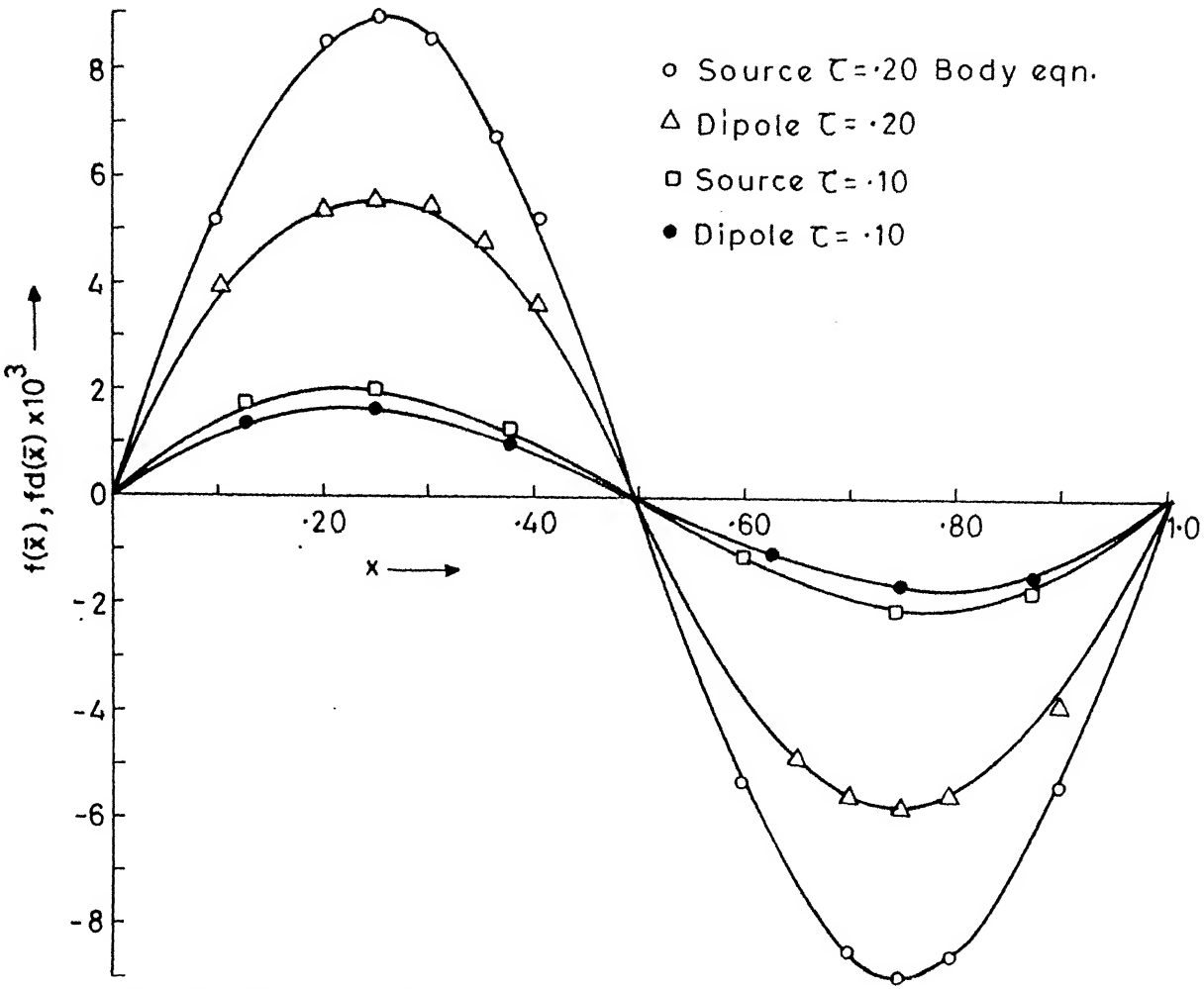

Fig.10 Strength distbn. of source & dipole PR=1·1

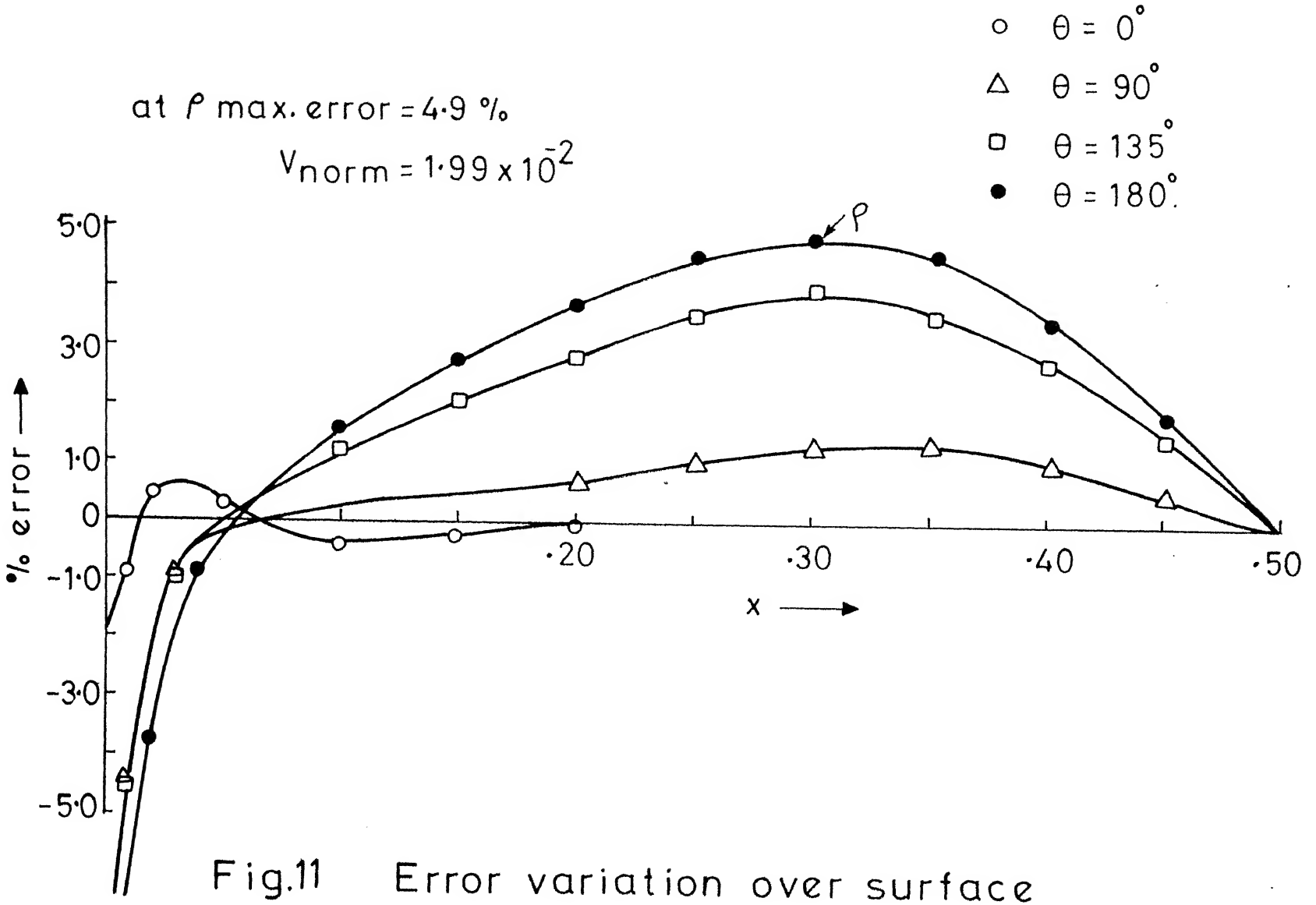

Fig.11 Error variation over surface

$C_1 = C_2 = \cdot 2$, PR = 1·1

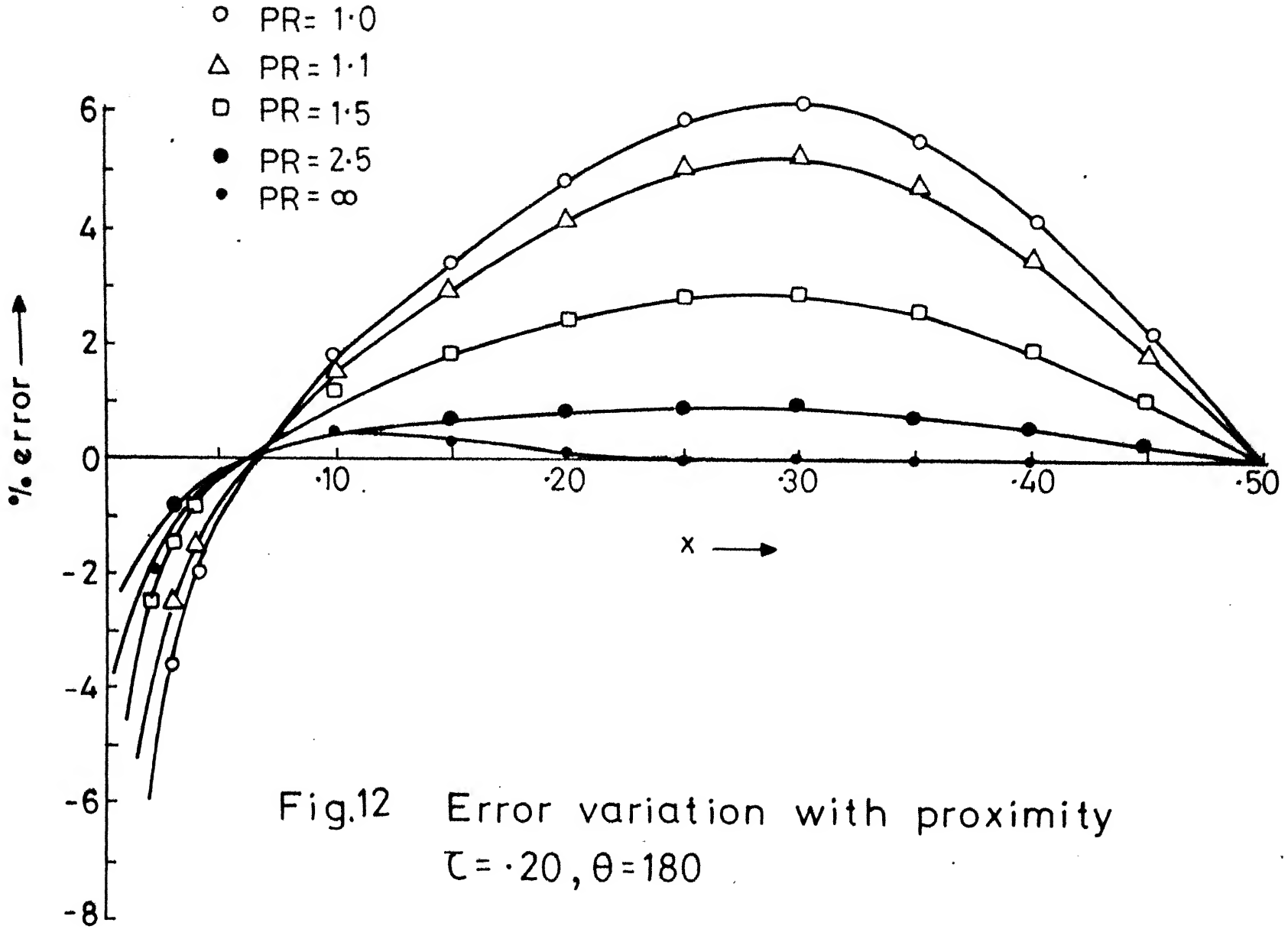

Fig.12 Error variation with proximity
$\tau = \cdot 20, \theta = 180$

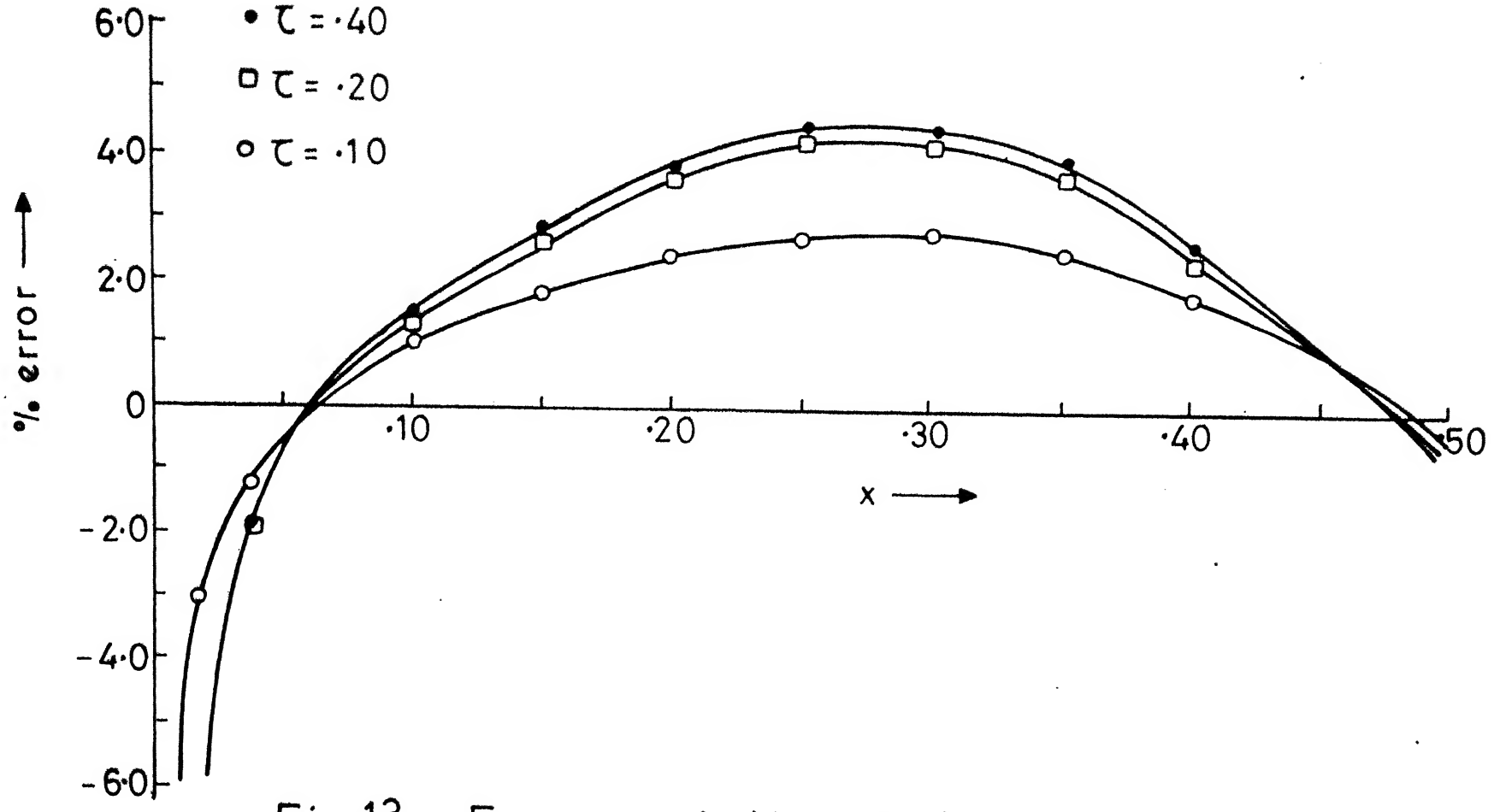

Fig.13 Error variation with thickness
PR = 1·1, θ = 180°

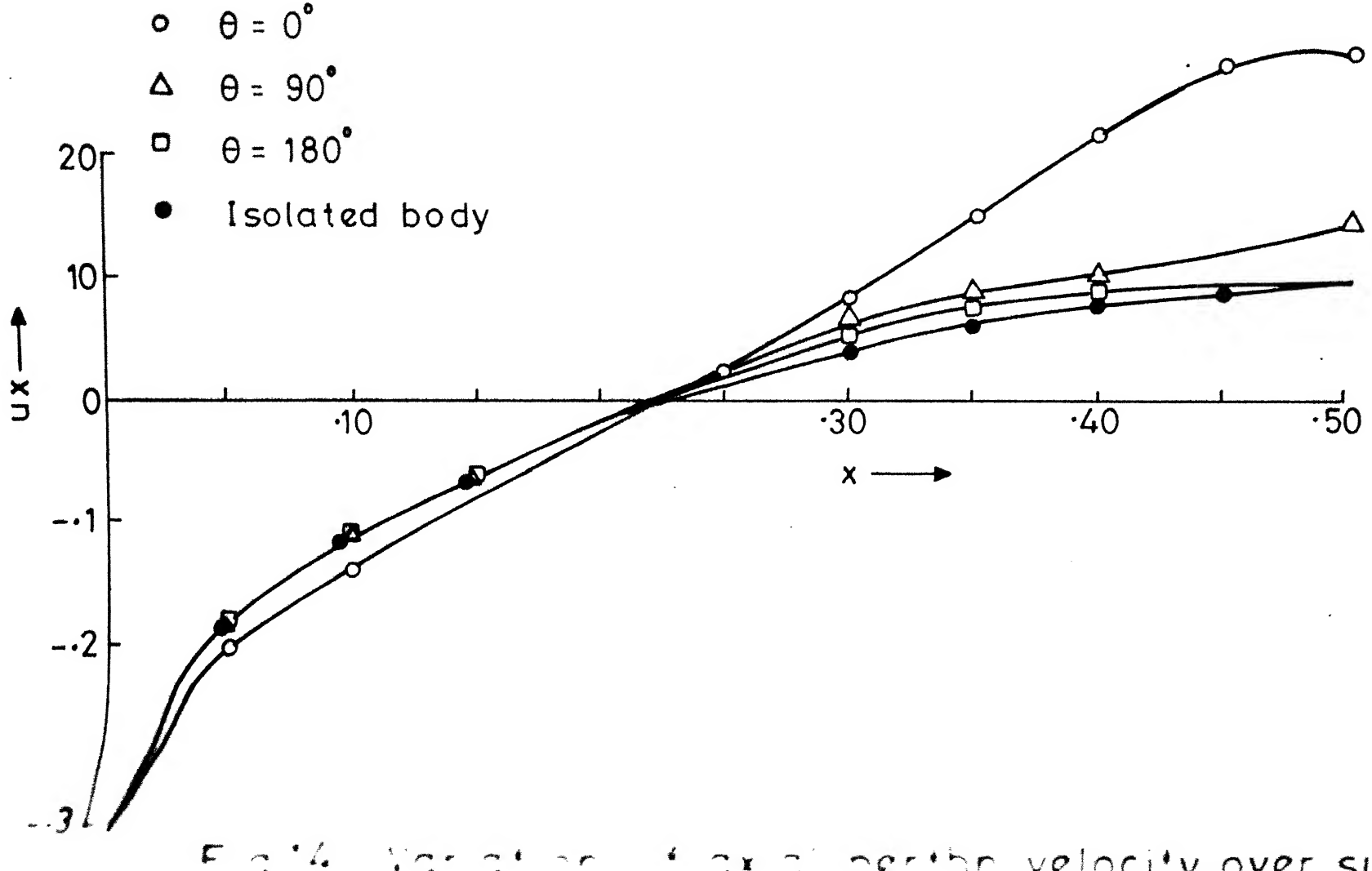

Fig. 4. Variation of axial perturbation velocity over surface

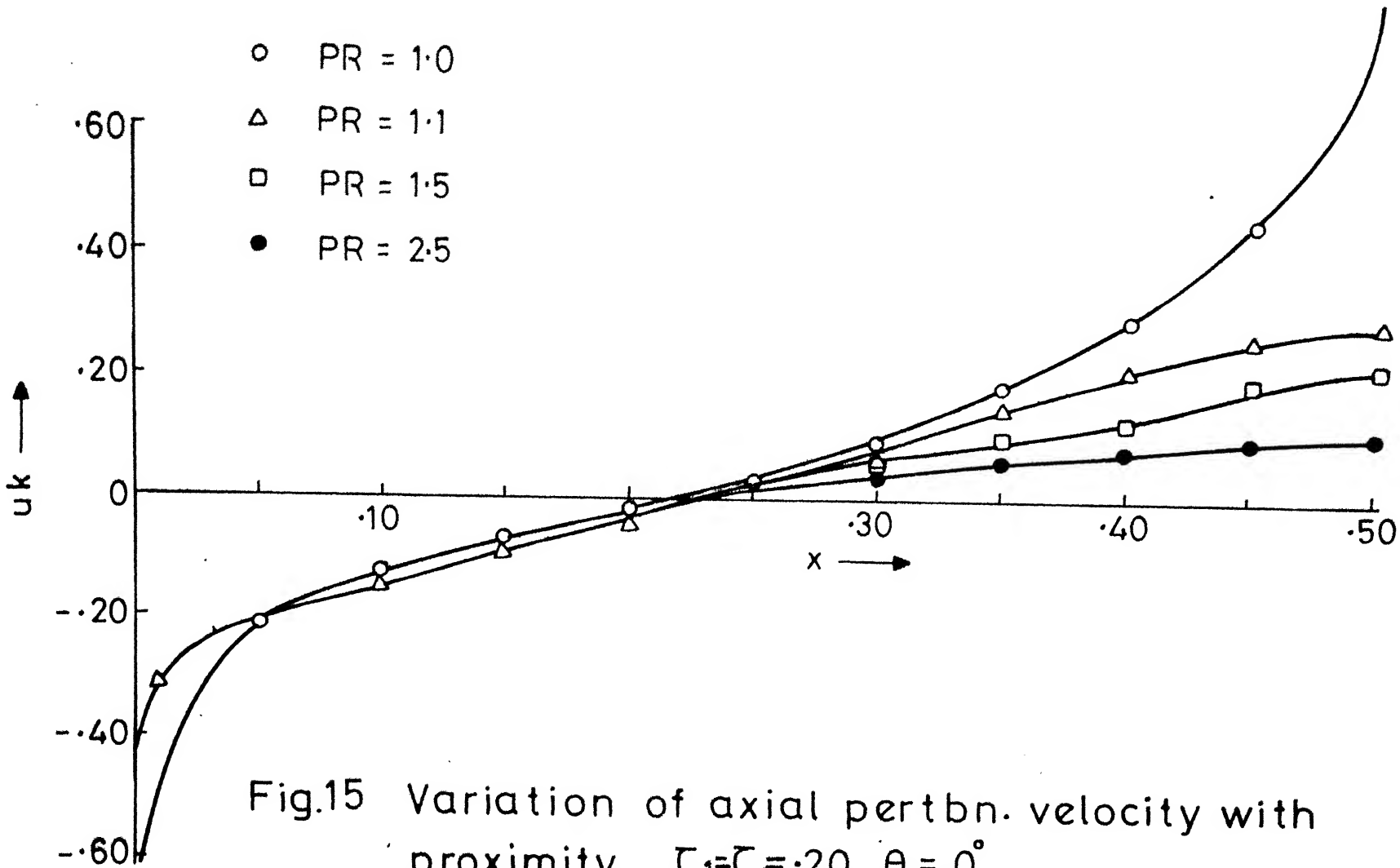

Fig.15 Variation of axial pertbn. velocity with proximity $\tau_1=\tau_2=\cdot 20$, $\theta = 0^\circ$

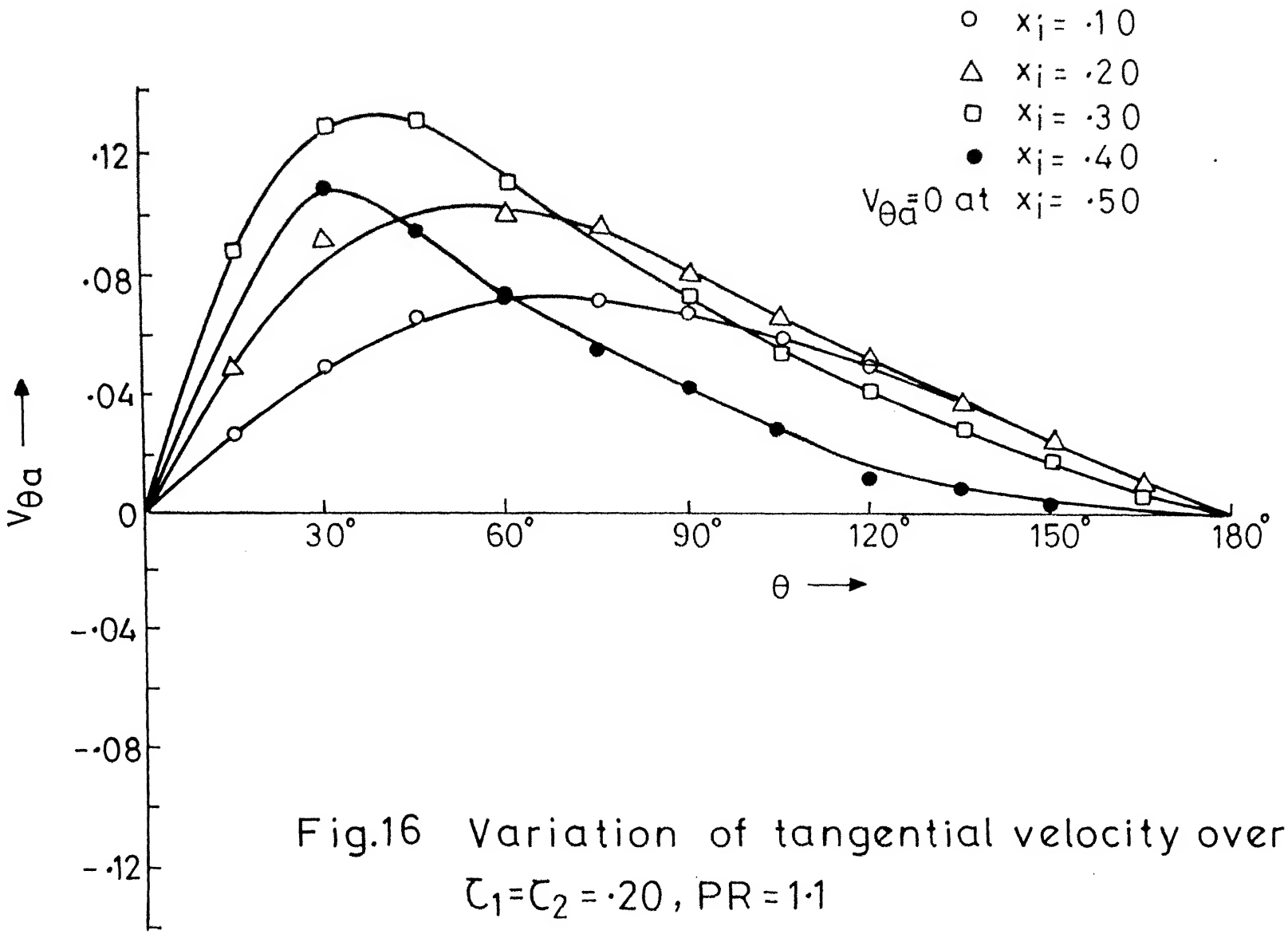

Fig.16 Variation of tangential velocity over surface

$C_1 = C_2 = ·20$, PR = 1·1

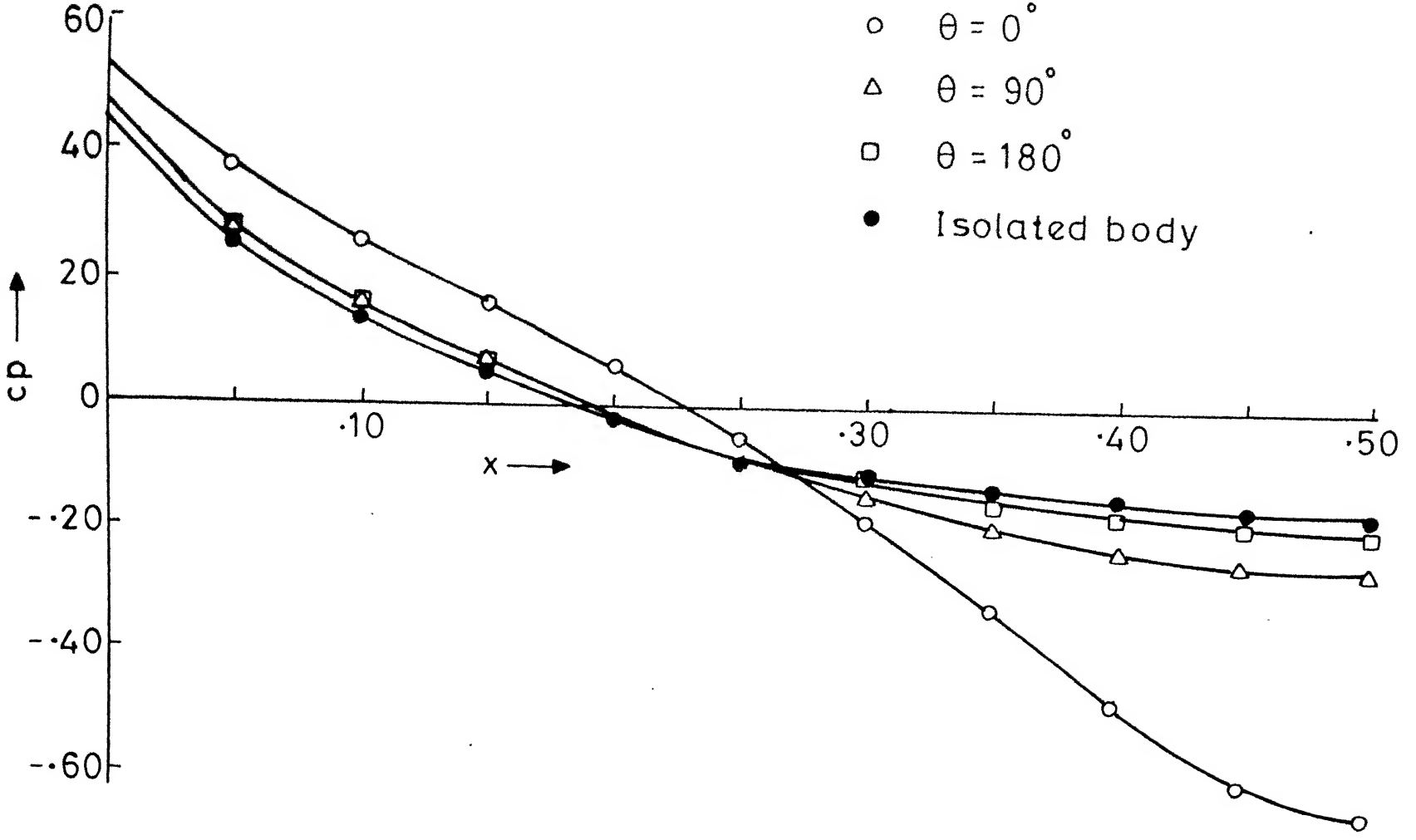

Fig.17 Distribution of pressure co-efficient on surface
$\tau_1 = \tau_2 = \cdot 20$, PR = 1·1

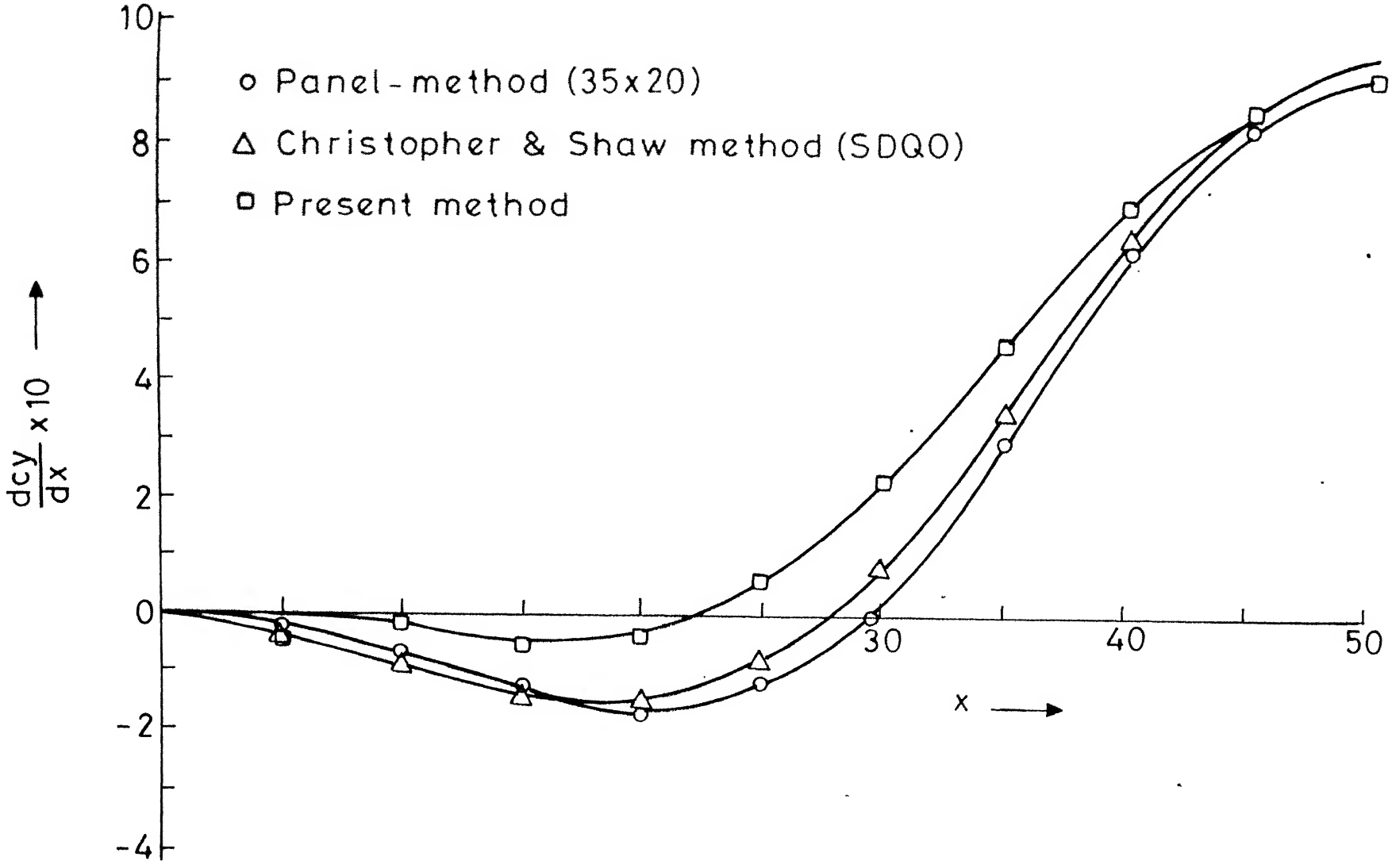

Fig.18 Side load distribution with x in axial flow

$\tau_1 = \tau_2 = \cdot 20$, PR = 1.1

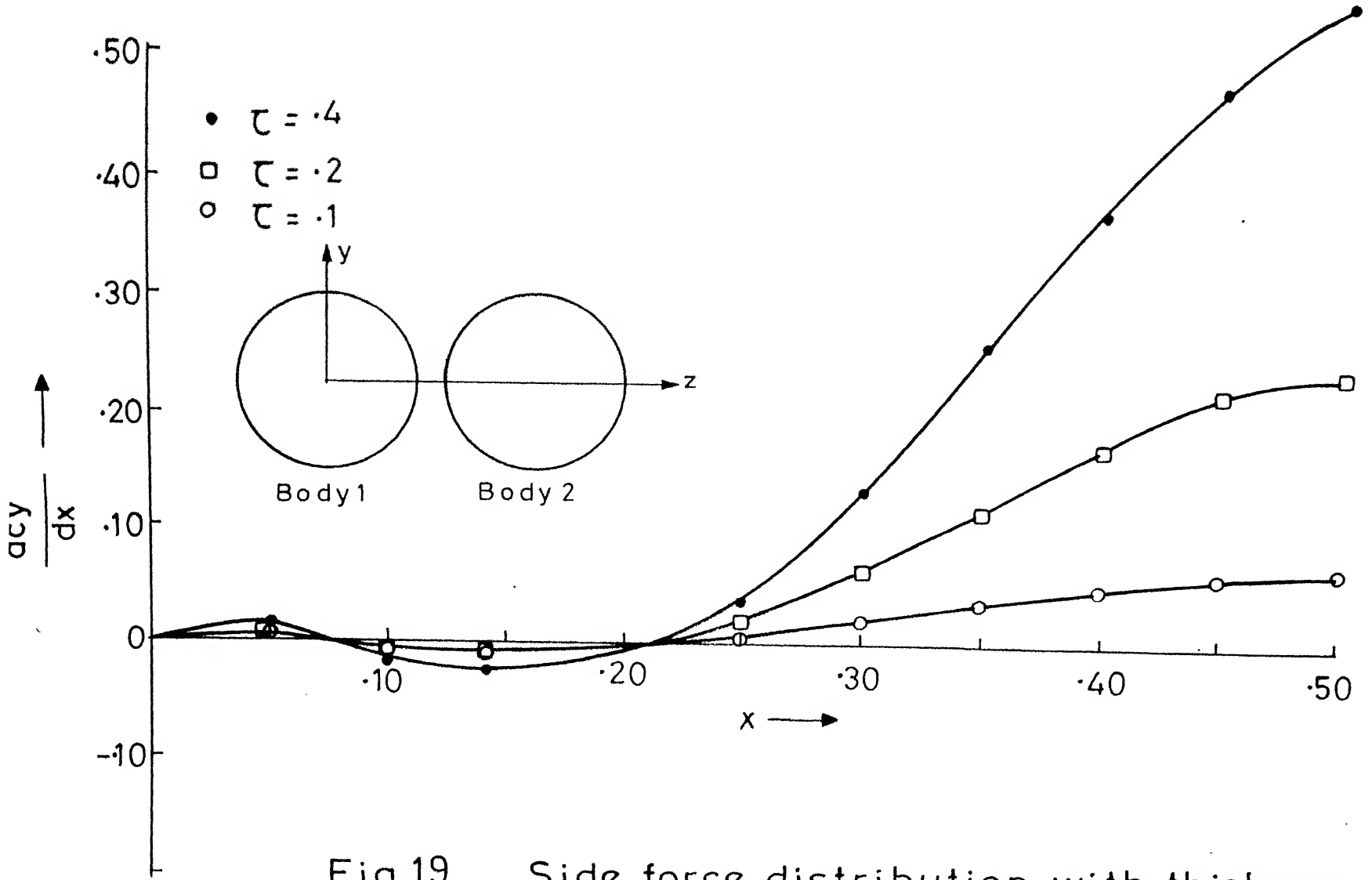

Fig.19 Side force distribution with thickness

PR=1·1

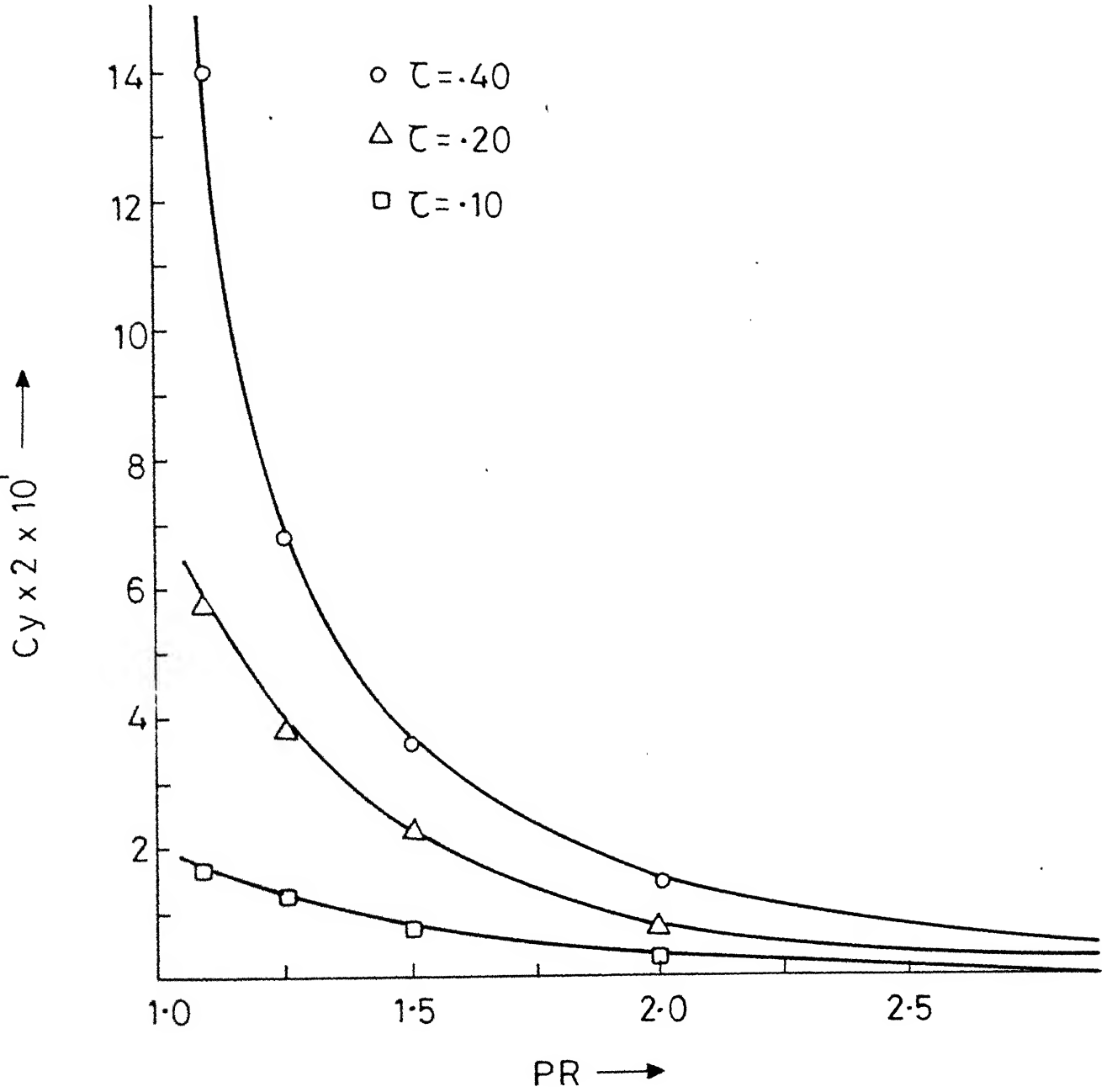

Fig.20 Variation of side force coefficient with proximity and thickness

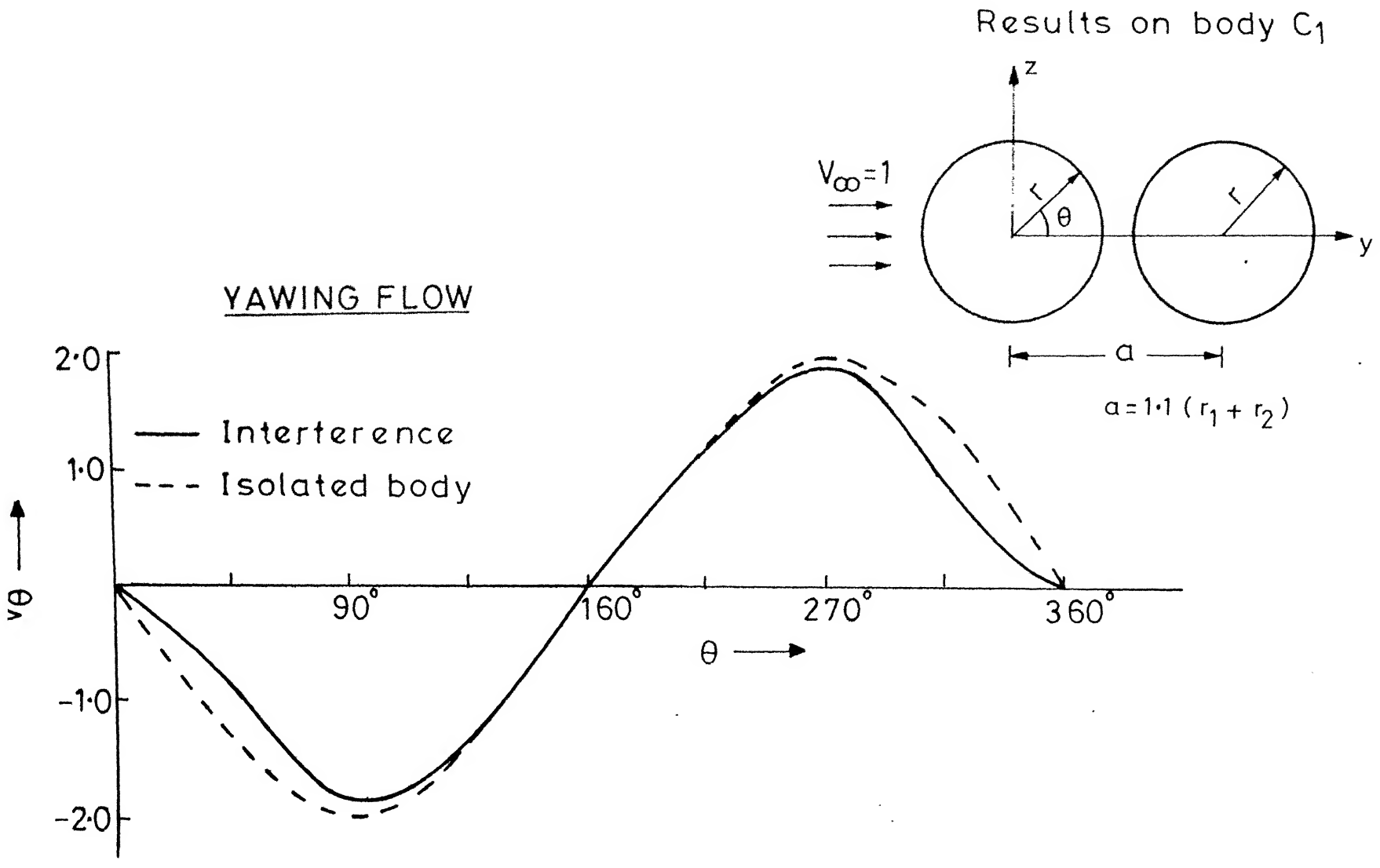

Fig.21 Variation of tangential velocity with θ

$r_1 = r_2$, PR = 1·1

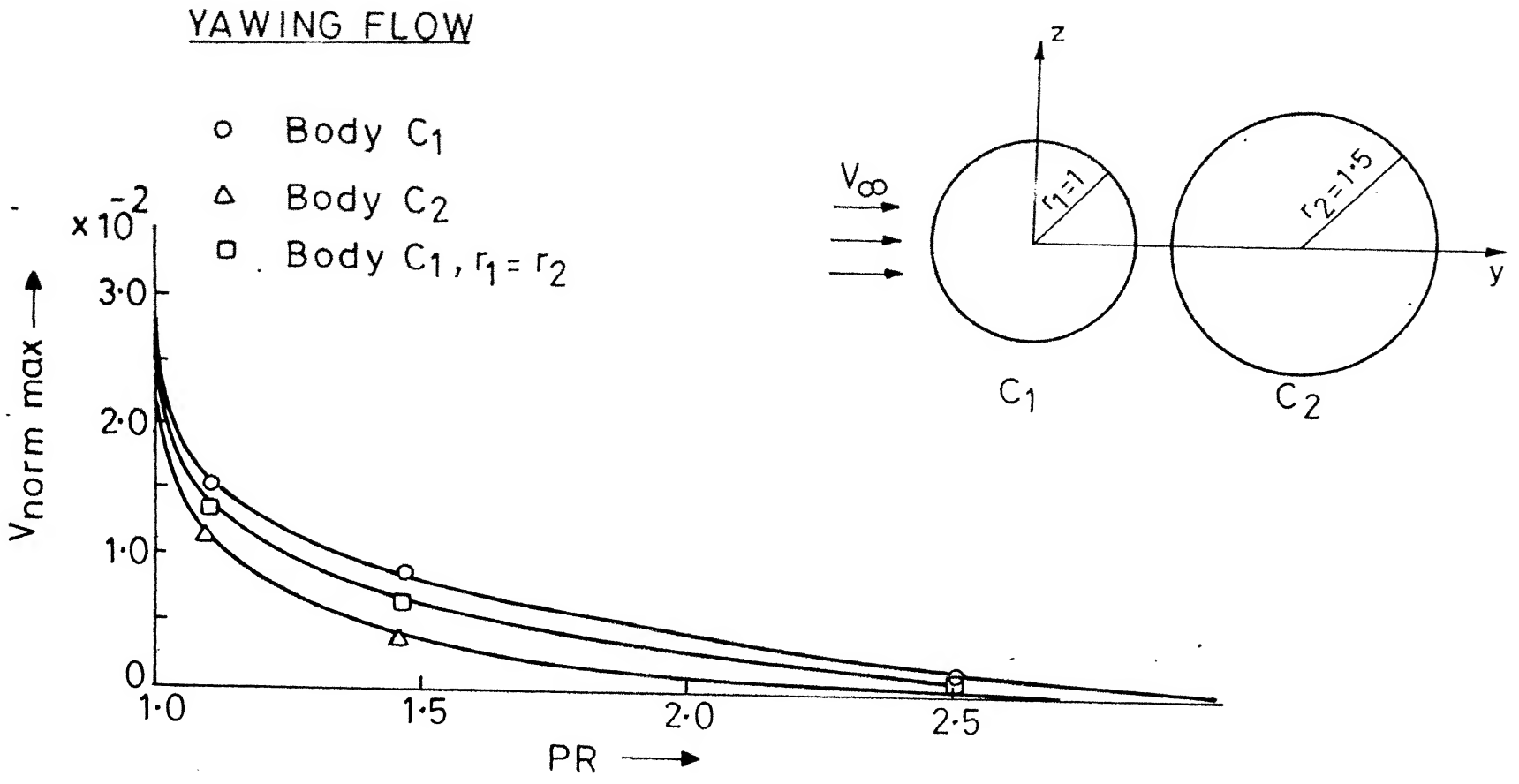

Fig.22 Error variation with proximity

$V_{norm} = V_r$ = Error

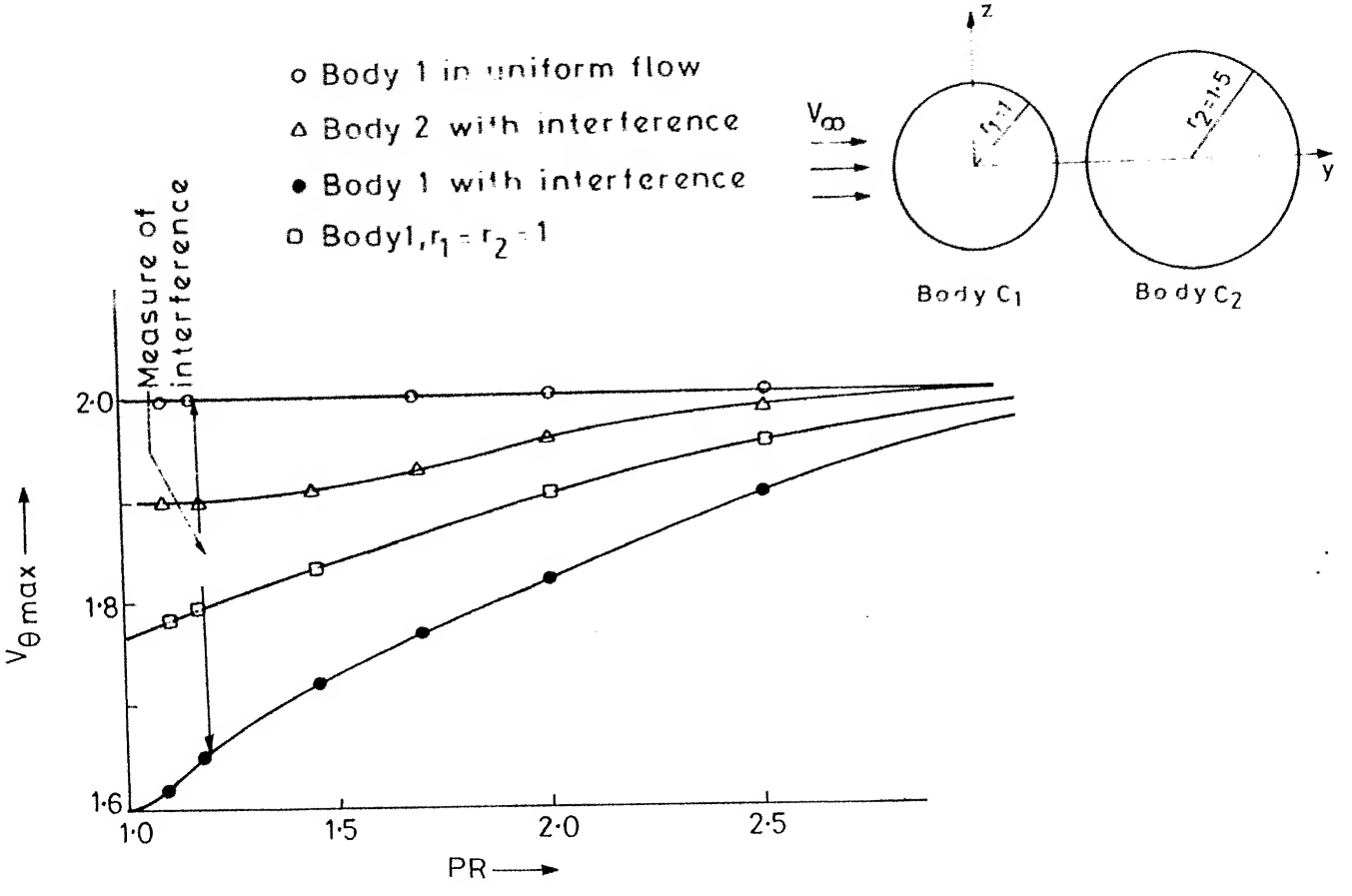

Fig.23 Variation of maximum tangential velocity with proximity

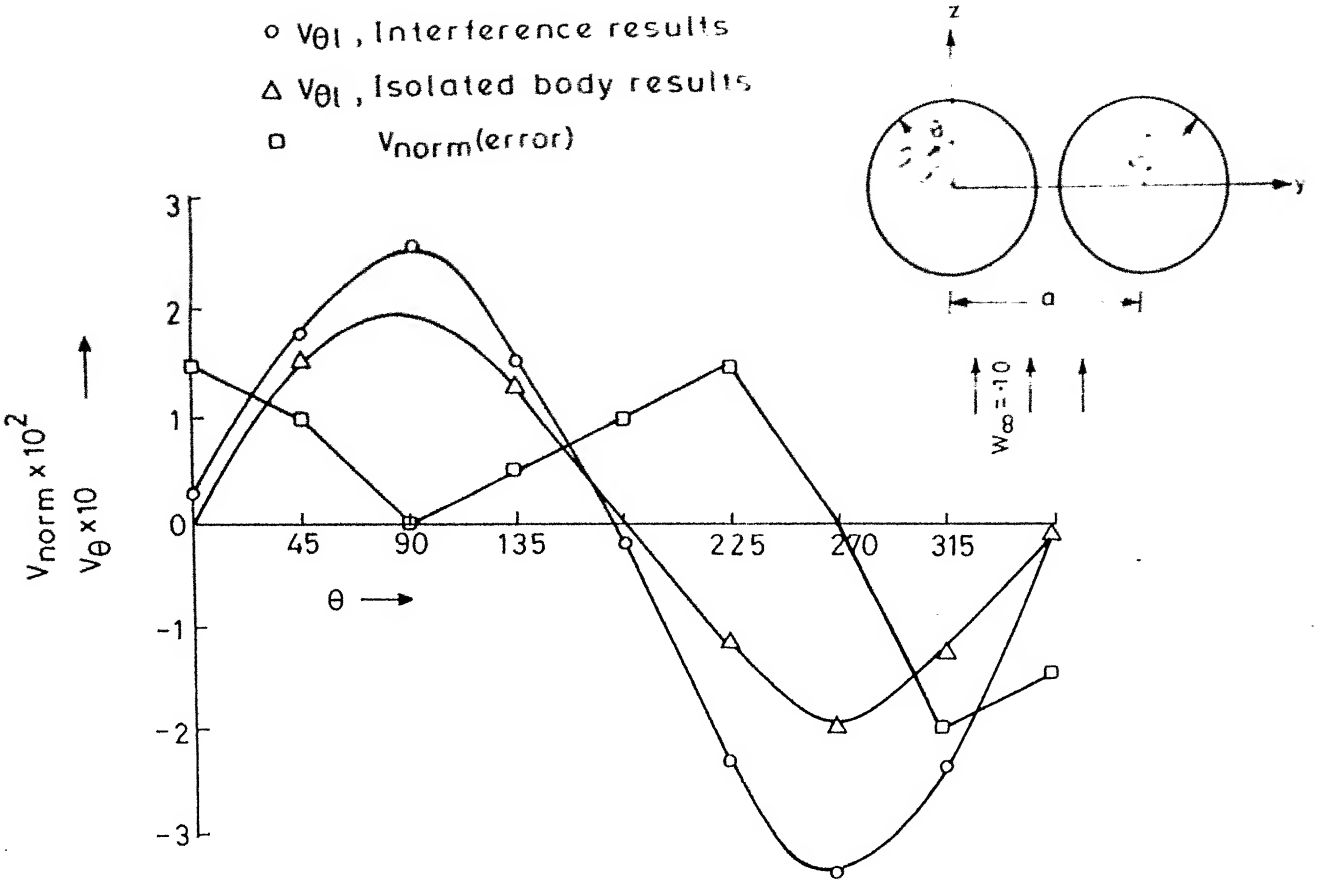

Fig.24 Variation of V_θ and V_{norm} with θ

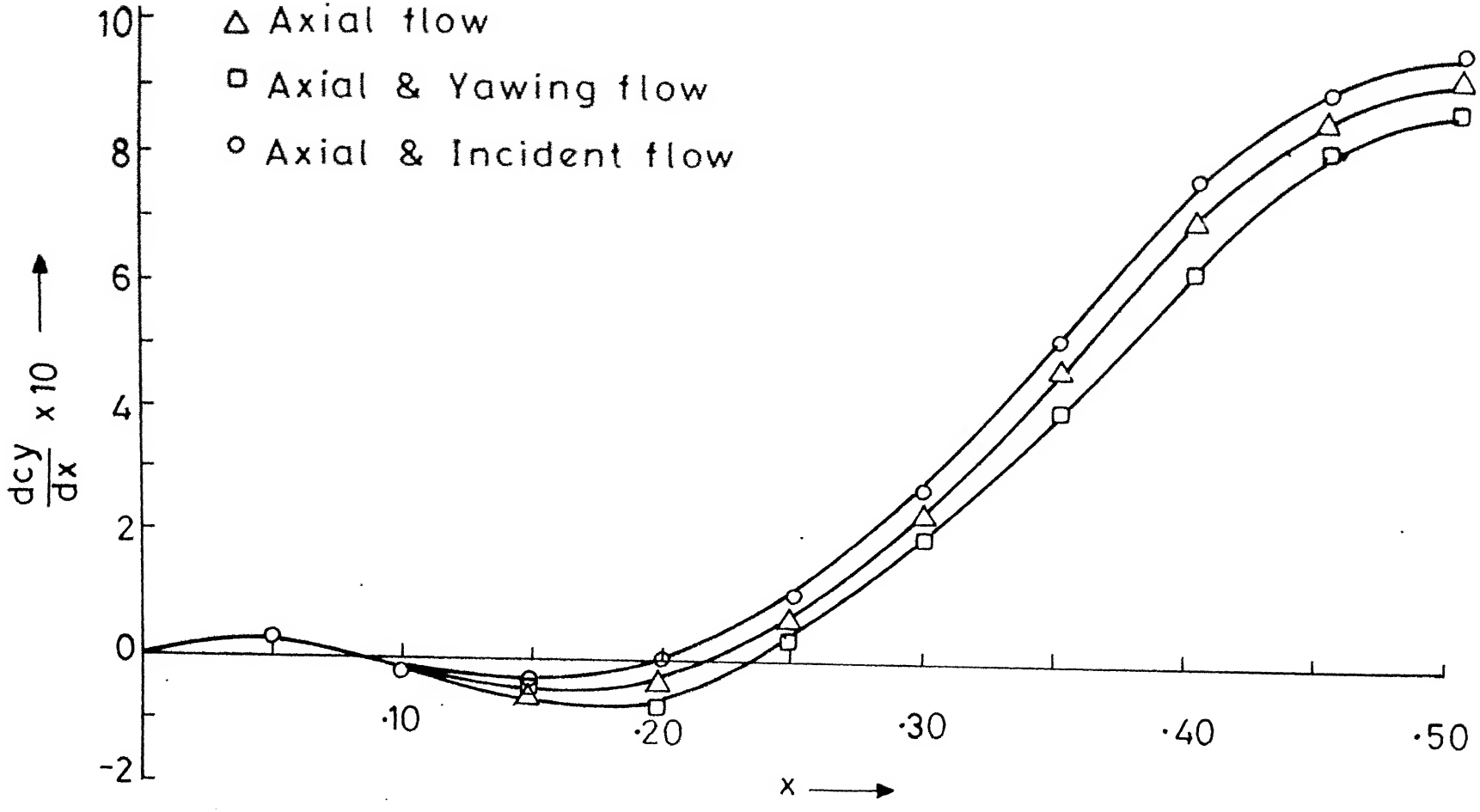

Fig.25 Axial and lateral flow combined

$\tau_1 = \tau_2 = \cdot 20$, PR = 1·1